SANDIA REPORT
SAND2021-12691
Printed October 2021

Sandia National Laboratories

Assessment of Electrode Contamination Mitigation at 0.5 MA Scale

Derek C Lamppa, Sean C. Simpson, Brian T. Hutsel, George R. Laity, Michael E. Cuneo
Sandia National Laboratories
P.O. Box 5800, MS-1195
Albuquerque, NM 87185
dclampp@sandia.gov

David V. Rose
Voss Scientific, 418 Washington St. SE,
Albuquerque, NM 87108

Prepared by
Sandia National Laboratories
Albuquerque, New Mexico
87185 and Livermore,
California 94550

Issued by Sandia National Laboratories, operated for the United States Department of Energy by National Technology & Engineering Solutions of Sandia, LLC.

Available to DOE and DOE contractors from
U.S. Department of Energy
Office of Scientific and Technical Information
P.O. Box 62
Oak Ridge, TN 37831

Telephone: (865) 576-8401
Facsimile: (865) 576-5728
E-Mail: reports@osti.gov
Online ordering: http://www.osti.gov/scitech

Available to the public from
U.S. Department of Commerce
National Technical Information Service
5301 Shawnee Rd
Alexandria, VA 22312

Telephone: (800) 553-6847
Facsimile: (703) 605-6900
E-Mail: orders@ntis.gov
Online order: https://classic.ntis.gov/help/order-methods/

ABSTRACT

The Z Machine at Sandia National Laboratories uses current pulses with peaks up to 27 MA to drive target implosions and generate high energy density conditions of interest for stockpile stewardship programs pertinent to the NNSA program portfolio. Physical processes in the region near the Z Machine target create electrode plasmas which seed parasitic current loss that reduce the performance and output of a Z experiment. Electrode surface contaminants (hydrogen, water, hydrocarbons) are thought to be the primary constituent of electrode plasmas which contribute to loss mechanisms. The Sandia team explored *in situ* heating and plasma discharge techniques by integrating requisite infrastructure into Sandia's Mykonos LTD accelerator, addressing potential impacts to accelerator operation, and reporting on the impact of these techniques on electrode plasma formation and shot performance. The i*n situ* discharge cleaning utilizes the electrodes of the accelerator to excite an argon-oxygen plasma to sputter and chemically react contaminants from electrode surfaces. Insulating breaks are required to isolate the plasma in electrode regions where loss processes are most likely to occur. The shots on Mykonos validate that these breaks do not perturb experiment performance, reducing the uncertainty on the largest unknown about the *in situ* cleaning system. Preliminary observations with electrical and optical diagnostics suggest that electrode plasma formation is delayed, and overall inventory has been substantively reduced. *In situ* heating embeds cartridge heaters into accelerator electrodes and employs a thermal bakeout to rapidly desorb contaminants from electrode surfaces. For the first time, additively manufactured (AM) electrode assemblies were used on a low impedance accelerator to integrate cooling channels and manage thermal gradients. Challenges with poor supplier fabrication to specifications, load alignment, thermal expansion and hardware movement and warpage appears to have introduced large variability in observed loss, though, preventing strong assertions of loss reduction via *in situ* heating. At this time, an *in situ* discharge cleaning process offers the lowest risk path to reduce electrode contaminant inventories on Z, though we recommend continuing to develop both approaches. Additional engineering and testing are required to improve the implementation of both systems.

.

ACKNOWLEDGMENTS

We could not have completed the work summarized in this report without the support of the team responsible for Mykonos. Adam Steiner, Jim Moore, Kate Bell, and Mark Kiefer immensely helped with machine operation, turnaround, scheduling, and contending with the safety paperwork associated with the hazards of our subsystems. A special thanks goes to co-author Brian Hutsel for training Derek Lamppa to act as a Mykonos shot operator.

We thank Robert Obregon for his tireless efforts to load, unload, and refurbish the Mykonos vacuum chamber between shots. His enthusiasm, hard work, and willingness to work late nights enabled multiple shots in a day more than once.

Larry Lucero and his RAMP facility were critical to the success of the parallel plate platform for *in situ* discharge cleaning. He modified shot hardware, built prototypes, insulating breaks, electronics chasses, and too many one-off fixturing components to list here.

We thank Drew Johnson for helping dust off the old PISCES controller and updating the software and hardware to be compatible with operations at Mykonos.

Karen DeZetter was absolutely essential during the *in situ* heating shot series, and we are very grateful for her patience and persistence through engineering challenges, shots successful or otherwise, and shot series hardware setup and teardown.

A special thanks to Susan Ossareh for her involvement in establishing the alignment process used for accurate measurements to fractions of a milli-radian for the *in situ* heating load components on Mykonos.

We thank David Saiz and Chuck Walker for their assistance on the *in situ* heating platform.

We are grateful the attention of the power flow topical area and meeting attendees who listened to our regular updates. Conversations on diagnostics and inspirational ideas were commonplace with Sonal Patel, David Yager-Elorriaga, Gabriel Shipley, Clayton Myers, Matt Gomez, Andy Porwitzky, Mark Johnston, Mark Hess, Charles Rose, and many others.

Additionally, the authors are grateful for the enlightening discussions, encouragement, and continued support of (attributed co-authors) Mike Cuneo and George Laity, and with Keith Matzen.

Sandia National Laboratories is a multi-mission laboratory managed and operated by National Technology and Engineering Solutions of Sandia LLC, a wholly owned subsidiary of Honeywell International Inc. for the U.S. Department of Energy's National Nuclear Security Administration under contract DE-NA0003525. This report describes objective technical results and analysis. Any subjective views or opinions that might be expressed in the report do not necessarily represent the views of the U.S. Department of Energy or the U.S. Government.

CONTENTS

LIST OF FIGURES

LIST OF TABLES

EXECUTIVE SUMMARY

The Z Machine at Sandia National Laboratories uses current pulses with peaks up to 27 MA to drive target implosions and generate high energy density conditions of interest for stockpile stewardship programs pertinent to the NNSA program portfolio. Physical processes in the region near the Z Machine target create electrode plasmas which seed parasitic current loss that reduce the performance and output of a Z experiment. The Advanced Diagnostics program is supporting power flow research on the Z facility. We are actively pursuing methods to both simulate and experimentally observe these parasitic loss mechanisms. We are also interested in identifying sources of parasitic current loss and defining technologies and material processes that can mitigate, reduce, delay, or eliminate their effect on power transmission to the Z target. We employ analytic theory, particle-in-cell simulations, and experiments on the Z and Mykonos accelerators to validate the effect of current loss mechanisms, and to develop methods to delay or eliminate these phenomena. Such efforts will provide improved performance for all experiments on Z, as well as bolster confidence in the design of a next-generation, 60-MA-class pulsed power accelerator facility.

Our AD Level-2 Milestone for FY21 (MRT 7291) was to evaluate technology options that mitigate electrode contaminants on a 0.5-MA-class low impedance accelerator. Electrode contaminants (hydrogen, water, hydrocarbons) are thought to be the primary constituent of electrode plasmas which contribute to parasitic loss mechanisms. The Sandia team was to explore *in situ* heating and plasma discharge techniques by integrating requisite infrastructure into the Mykonos accelerator, address potential impacts to accelerator operation, and report on the impact of these *in situ* techniques on electrode plasma formation and power flow. This document summarizes that work.

In situ discharge cleaning utilizes the electrodes of the accelerator to excite an argon-oxygen plasma to sputter and chemically react contaminants from electrode surfaces. Insulating breaks are required to isolate the plasma in electrode regions where loss processes are most likely to occur. The shots on Mykonos validate that these breaks do not perturb experiment performance, reducing the uncertainty on the largest unknown about the *in situ* cleaning system. A two-stage, 90-minute cleaning process has demonstrated very encouraging results. Preliminary observations with electrical and optical diagnostics suggest that electrode plasma formation is delayed, and overall inventory has been substantively reduced. Opportunities are abundant for continued work in this area. The plasma cleaning results are particularly promising and are motivating several shot campaigns on Mykonos in FY22 as well as light lab experiments. Continued experiments will attempt to define optimized cleaning plasma conditions as a function of electrode spacing and cleaning plasma excitation parameters.

In situ heating embeds cartridge heaters into accelerator electrodes and employs a thermal bakeout to rapidly desorb contaminants from electrode surfaces. For the first time, additively manufactured (AM) electrode assemblies were used on Mykonos to integrate cooling channels and manage thermal gradients. Previous experimental results and experience with vacuum chamber pre-conditioning suggest that a properly applied bakeout process can reduce observed current loss below unheated experimental references. Challenges with poor supplier fabrication to specifications (e.g. out of concentricity anodes), load alignment, thermal expansion and hardware movement and warpage appears to have introduced large variability in observed loss, though, preventing strong assertions of loss reduction via *in situ* heating. Concerns about thermal expansion and subsequent permanent

warpage of electrodes contribute to the assessment that *in situ* heating is the more challenging system to implement on Z. The number of experiments we could execute was limited by supplier production of our complex assemblies during COVID. However, our experiments were sufficient to identify the outstanding engineering challenges.

At this time an *in situ* discharge cleaning process offers the lowest risk path to reduce electrode contaminant inventories on Z. Ultimately, discharge cleaning can reduce electrode surface contamination, while heating can reduce both electrode surface and bulk contamination. Both techniques elevate electrode temperatures to prevent recontamination prior to an accelerator's downline shot. We recommend continuing to develop both approaches. Additional engineering and testing are required to improve the implementation of both systems.

1. INTRODUCTION

1.1. Background

Large pulsed power accelerators, such as the Z Machine, routinely deliver current pulses on the order of 25-27 MA to a variety of physics experiments of interest to national security science programs [1]. This current is delivered to an inductive load through four parallel Magnetically Insulated Transmission Lines (MITLs) which are then combined into a single MITL using geometric current adders in the double post-hole convolute. An example geometry of the Z Machine is shown in Figure 1 [2]. The inner MITL and the anode posts experience the highest current density in the pulsed power system, which results in extreme ohmic heating and particle bombardment of the electrode surfaces. Rapid heating of the electrodes causing flash desorption of surface and bulk contaminants when temperatures exceed ~ 400°C [3]. In turn, this desorbed neutral gas is subsequently ionized leading to plasma formation on electrodes, which we believe contributes to several parasitic current loss mechanisms. We observe current loss up to 4 to 6 MA in certain high inductance load configurations. Direct spectroscopic measurements of the time-varying plasma suggest a correlation between observed current loss and cathode plasma expansion, a plasma that appears to be dominated by hydrogen [4]. This is most likely the result of physisorbed and chemisorbed contaminants such as molecular water (H_2O), hydrogen (H_2), hydrocarbons (C_xH_y), hydroxyls (-OH), nitrides, and oxides present on the electrode surface [5]. A visualization of this contaminant overlayer on the bare substrate is depicted in Figure 2.

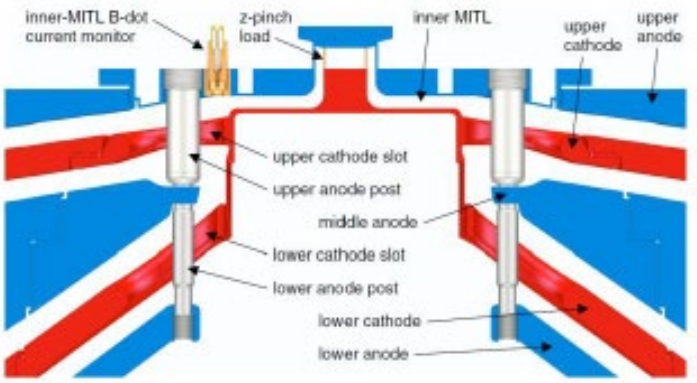

Figure 1: Cross-sectional view of a Z accelerator convolute used for HED physics experiments [2]. Current loss is believed to be confined within the high-energy regions of the convolute posts and in the Inner MITL.

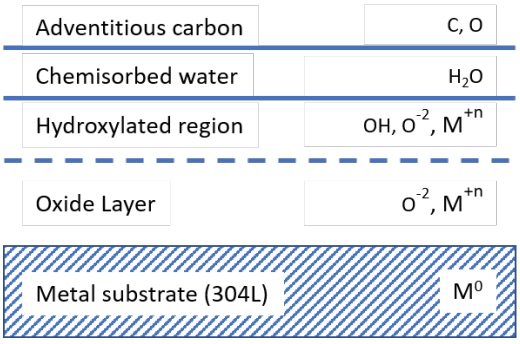

Figure 2: Illustration of the typical contaminants present on 304L stainless steel under high vacuum [5].

A better understanding of plasma formation on 'real' electrode materials and the development of methods for reducing the rapid neutral desorption of contaminant inventories is necessary to improve current delivery on today's accelerators and may provide a scalable path forward to NGPP architectures of the future. Two approaches were investigated to help understand and demonstrate the efficacy of *in vacuo* treatments of power-flow surfaces. The first approach employed (i) *in situ* plasma discharge cleaning of an optically accessible geometry; the second approach investigated (ii) *in situ* heating of the anode and cathode either independently or combined.

In situ heating and plasma discharge cleaning processes enjoy a robust history with prolific publications showing use for vacuum chamber pre-conditioning, tokamak conditioning, and improving performance of high-impedance vacuum diodes. References to this literature will be made in subsequent sections when appropriate. The employment of these processing techniques is

novel in that we are attempting to improve current delivery of low impedance (<1 Ω) high current accelerators, whereas previous work focused on vacuum diodes with initial impedances ~20-200Ω. Published figures of merit important to high-impedance vacuum diodes like gap closure and impedance collapse are not fully analogous to the extremely high magnetic field environments of multi-MA accelerators like those found in the Z convolute and inner MITL. This report summarizes the first steps to improve our scientific understanding of the effect of *in situ* treatment on plasma dynamics in low-impedance MITLs, correlate how these changes further influence observed parasitic current loss, and develop engineered systems to be deployed to the Z Machine to improve shot reliability and performance.

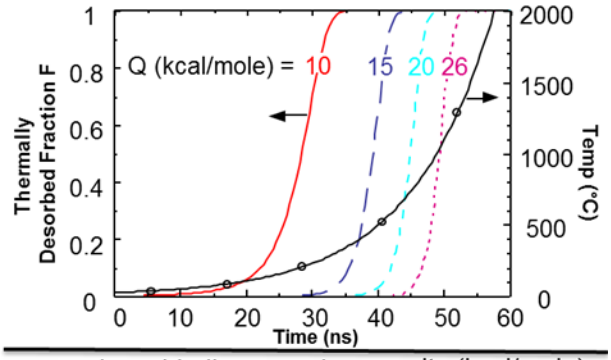

contaminant binding energies	units (kcal/mole)
Physisorbed contaminants:	Q ≈ 2 - 14
all gases (except H_2O)	Q ≈ 2 - 10
H_2O	Q ≈ 8 - 14
Chemisorbed contaminants:	Q ≈ 10 - 50
C_nH_m	Q ≈ 20 - 30
H_2 (various metals)	Q ≈ 10 - 40
H_2 (stainless)	Q ≈ 21
stain. outgas. charac.	Q ≈ 22 - 25
CO (on stainless)	Q ≈ 22 - 47
oxide layers:	Q ≈ 50 - 100

Figure 3: Fractional desorption of inventories of various binding energies during an example rapid pulse-heating of an electrode; lightly bound contaminants are quickly desorbed (top). Sample binding energies for physisorbed and chemisorbed molecules (bottom) [6].

Figure 3 provides a physical description of the process of desorption in a pulsed power system. The populations of surface contaminants identified in Figure 2 are bound to the surface with a characteristic quantity known as binding energy; inspection of the bottom table shows a survey of light atom species containing H, C, and O have binding energies below 30 kcal/mol. Current pulses like those in the Z convolute and inner MITL will quickly heat the surface of the electrode. The top graph in Figure 3 shows in black a notional exponentially-increasing heating profile. The graph shows that that surface contaminants with binding energies below 30 kcal/mol will be completely desorbed within 50-60ns on an electrode heated to 500°C in roughly 40 ns. This heating profile is notionally feasible in low-impedance accelerator MITLs for electrodes with high lineal current densities (e.g. regions exceeding 2 MA/cm) and has been achieved on the Mykonos platform in work summarized in this report (see Figure 10). Once desorbed, electric-field and collisional processes will quickly ionize these neutrals, at which point they are added to the electrode's plasma and subject to magnetohydrodynamic (MHD) processes thereon.

This L2 milestone was defined to document progress in these endeavors. The description for the scope of work for this milestone is to "Complete initial studies to evaluate technology options for mitigating electrode contaminants on 0.5-MA scale pulsed power accelerators." This work leverages Sandia's Mykonos-V Linear Transform Driver (LTD) as a low-cost surrogate for the assessment of electrode contamination mitigation studies at 0.5 – 1 MA scale. This report summarizes the experimental design and results of fielding *in situ* heating and cleaning processes on Mykonos downline pulses. We specifically address the systems' engineered designs, impact on accelerator operation, and discuss an assessment of technology readiness and next steps required to make these *in situ* process systems feasible on Z.

1.2. Organization of this Report

The remainder of this report is divided into four additional sections. Section 2 provides a brief overview of the Mykonos accelerator used for investigating *in situ* electrode conditioning processes. Section 3 is specific to *in situ* plasma discharge cleaning experiments and provides a general overview of the theory, the experimental configuration, and the results. Section 4 is specific to *in situ* heating experiments and follows the same format. And finally, Section 5 concludes the report and gives guidance as to the next steps for future work.

This page left blank

2. THE MYKONOS ACCELERATOR

The Mykonos Linear Transformer Driver (LTD) accelerator at Sandia allows us to field small scale (0.5-1 MA), high shot rate (1-3 times per day) experiments to evaluate the impact of *in situ* conditioning techniques on power flow in low impedance, high current transmission lines. Prior work has demonstrated the utility of electrode cleaning in higher impedance diodes with relatively large anode-cathode gaps of order 8-12-mm [6], [7]. However, the utility of electrode contamination control has never been demonstrated in low impedance, high current experiments. Our approach is to assess these conditioning techniques on a high shot rate accelerator with excellent diagnosability, and once proven, scale the approach towards a future capability to clean electrodes and improve electrical current delivery on the 20 MA Z accelerator.

The purpose of our Mykonos experiments is to evaluate the utility of *in situ* conditioning techniques for decreasing contaminant plasma formation and reduction of associated parasitic processes in low impedance systems. Small gap, high current, low impedance MITLs are a far more demanding environment, with electrodes quickly driven to temperatures sufficient for desorption. These MITLs could be sensitive to levels of contamination of order a few monolayers (1 monolayer [ML] is defined as 1e15 particles/cm^2).

The Mykonos LTD accelerator consists of five LTD cavities. These cavities are three meters in diameter, and each contains 36 bricks with two 40-nF capacitors that provide the electrical energy storage for the machine. These cavities can be operated at 100kV peak output and can deliver up to 1MA to a 0.5 Ω matched load [8]. A matched impedance to a nominal 15-20nH inductive load in the vacuum load region as shown in the following figure. The load platform developed for the *in situ* heating study is approximately 20-25nH, to which Mykonos will deliver about 850kA. The *in situ* discharge cleaning experimental hardware is approximately 35-40nH, reducing the delivered current to 650-750kA, depending on the parallel plate gap spacing and chosen electrodes. These new experimental platforms will be discussed in greater detail in subsequent sections of this report.

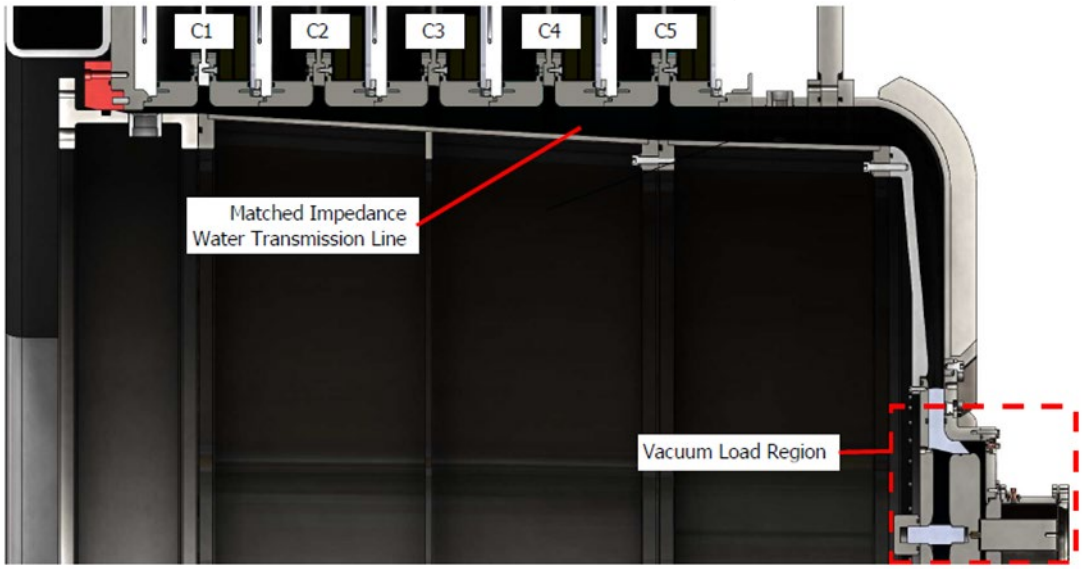

Figure 4: The Mykonos V LTD Module machine half section [8] showing a cross section of the five LTD cavities C1 through C5, the water-filled transmission line, and the vacuum load region located where experimental hardware is installed.

Figure 5 shows the locations of in-chamber current diagnostics that are referenced for both *in situ* heating and cleaning experimental campaigns. The upstream current probes are critical to assess current loss in an experiment because they are the final facility-calibrated measurement of the current pulse; differences from measurements here to the notional downstream current probes are defined to be current lost between the two measurements. In this image, the "MITL Experimental Gap" is where the loss should occur. Shown here is a 3mm cathode rod with a nominal 1mm anode-cathode (AK) gap [8], [9] and is the basis for the *in situ* heating experimental platform. Figure 6 shows sample results from these earlier studies with this configuration. The data plotted (Right) are example upstream and downstream currents for the indicated AK gap. The difference between upstream and downstream is current loss.

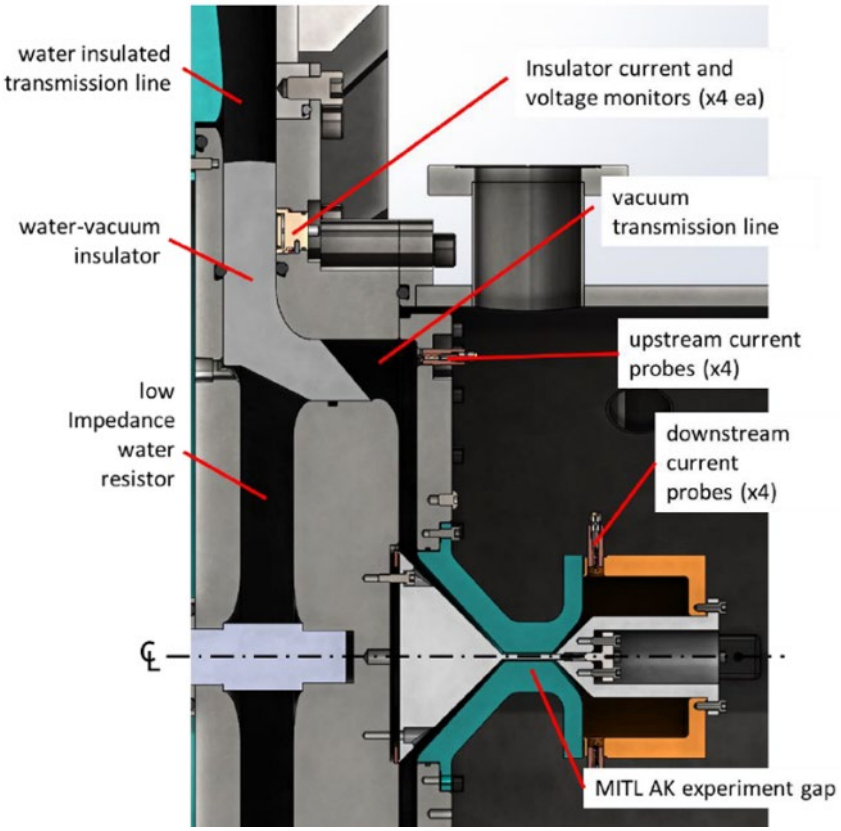

Figure 5: The Mykonos LTD accelerator load region [9]. Current flows to the right; experimental hardware is in the region labeled "MITL AK experiment gap."

We note one characteristic of the downstream current loss (red signals in Figure 6) is that it becomes constant at a time during the pulse, and that time occurs earlier for a smaller gap. The time at which the downstream current flatlines or "crowbars" is thought to be the time at which the anode and cathode plasmas cross the gap and merge, shorting out the current delivery to the downstream B-dots. The downstream current flatlines because the sensor is now measuring a long timescale L/R exponential decay of magnetic flux in the volume trapped between the short and the sensor. The upstream sensor signals see an apparent increase in current because the shorted MITL looks like a lower impedance. The time at which upstream and downstream current begin to diverge indicates when a loss process is beginning to dominate current flow in the load region.

The data shown on the left of Figure 6 shows that as AK gap increases in high current density MITLs, observed loss decreases. This initial data provides the starting point for the *in situ* heating platform.

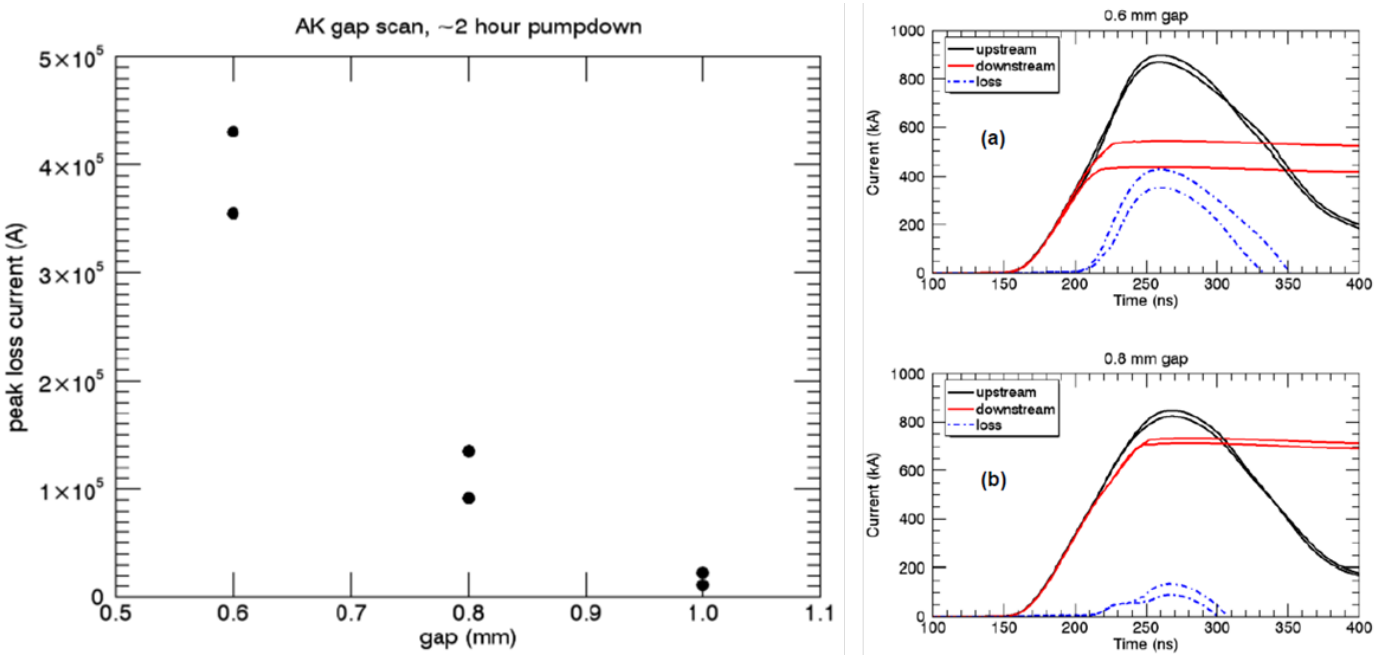

Figure 6: Earlier study of a high-current-density MITL [9] current profiles up- and down-stream of the experimental region (right). In (left), peak values of observed loss as a function of AK gap.

The Mykonos accelerator has become a robust collaborative environment for scientists, engineers, and diagnosticians to bring together their areas of expertise. Several facility capability improvements were implemented through a series of LDRD and SSAA investments since 2012, as well accelerator operations, pulsed power, and power flow activities supported by the Advanced Diagnostics sub-program. These collaborations over the past four years have significantly increased the diagnostic capabilities of the Mykonos facility, which now supports a broad portfolio of many different high energy density target physics, power flow, and pulsed power experiments. The data summarized in the previous figure represented the state of capabilities in 2014, namely electrical diagnostics only. Experimental teams have since incorporated a mounted optical table to the front to enable optical diagnostics including fast framing cameras, photodiode arrays, additional electrical channels, a four-frame pulsed laser shadowgraphy laser system, and other interferometric measurements (Figure 7).

The work completed under the scope of this project has contributed to a further increase in capability for Mykonos. We have designed and procured a new vacuum chamber to provide multiple optical lines of sight to experiments. To enable plasma cleaning protocols, we upgraded the vacuum system with pneumatic valving and remote/local controls and gauge readouts. We've incorporated additional electrical and gas infrastructure for *in situ* heating and discharge cleaning to enable these processes. Diagnostics supporting these processes have also been incorporated, for example a residual gas analyzer to observe desorbed contaminants and spectrometers to observe self-emission from cleaning plasma. These upgrades and new capabilities will pay dividends for future *in situ* conditioning experimental work in program outyears and will also benefit all future experimenters in the PF topical area and other pulsed power and HED research areas. There could

be opportunities to consider academic access that would have multiple benefits to Sandia, the Mykonos facility, to universities, and to NNSA programs.

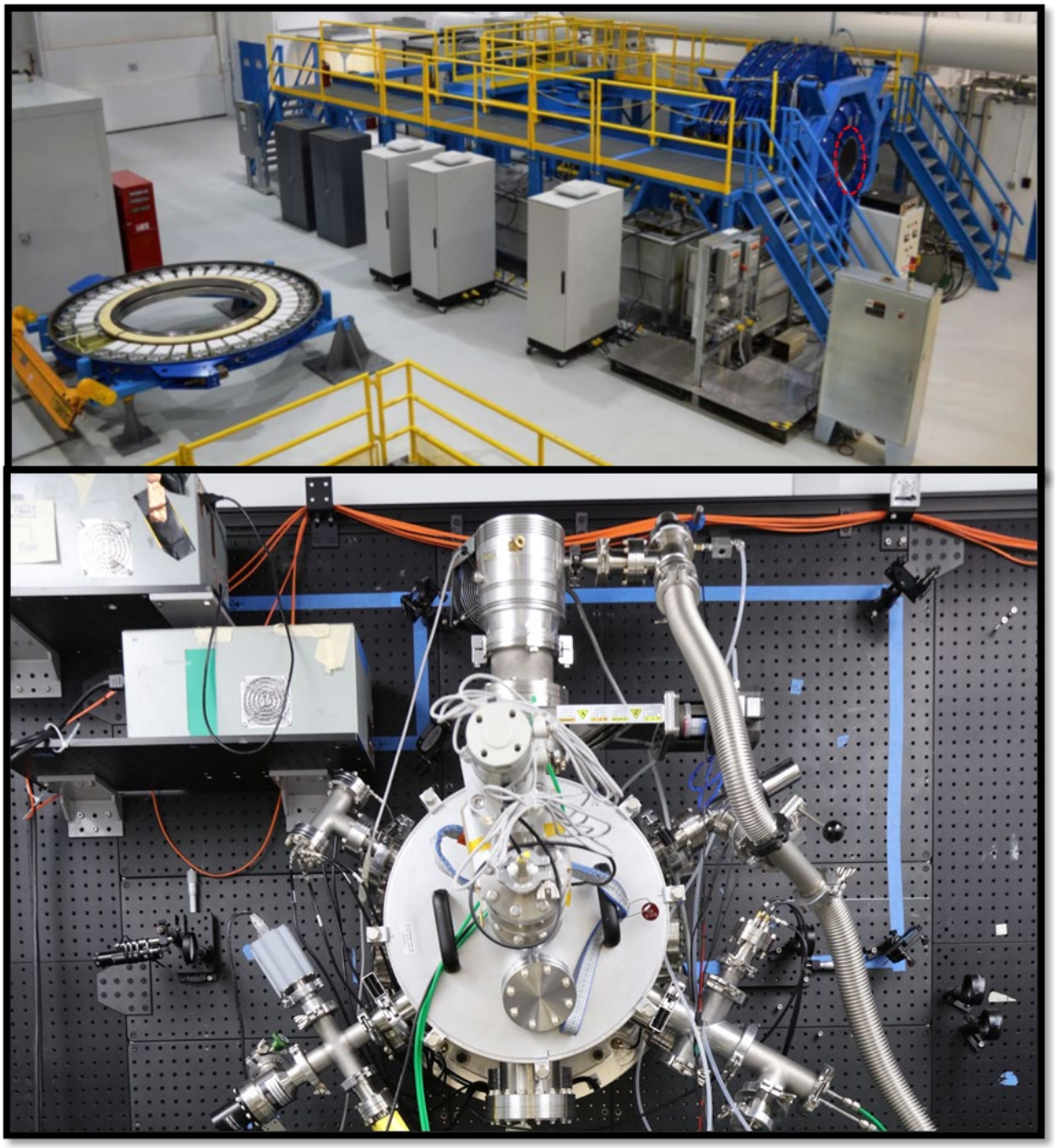

Figure 7: The Mykonos facility in 2014 (top) mounted load hardware and a vacuum chamber to the circled red region; only electrical diagnostics could be fielded. In 2021 (bottom), the *in situ* cleaning platform utilizes fast framing cameras, alignment lasers, photodiodes, remote/local control of vacuum pumping, and process gas plumbing and throttling of pumpout. The vacuum chamber "lid" visible in the middle of the bottom image (with two black handles) is roughly equivalent to the circled red region in the image from 2014.

3. *IN SITU* PLASMA DISCHARGE CLEANING

Plasma discharges can provide *in situ* electrode cleaning through bombardment of the electrode surfaces with plasma ions. Contaminants can be removed from metal electrodes through physical sputtering or chemically-enhanced gettering. For example, argon discharges with 20% oxygen show a factor of 5 times greater removal rate from surfaces compared to non-reactive discharge gases such as argon alone [10]**.** Discharges can be created via DC high voltages, via RF excitation (for example at 13.5 MHz), or via a process developed at Sandia referred to as Audio-Square-Wave (ASW) discharge with a 10 kHz frequency bipolar high voltage pulse train. RF discharges at up to 50-200 mTorr pressures can be set up in gaps as small as 5 – 10 mm relevant to gaps found in the convolute current adder on Z. ASW discharges at pressures of up to 1 Torr can be established in gaps as small as 0.5-1 mm, relevant to the inner transmission line on Mykonos or Z. Although there are tradeoffs between these two regimes, ASW discharges may have substantial utility for cleaning low impedance high current transmission lines with small AK gap. We are leveraging research of contamination characterization and removal with ASW discharges developed during the previous "Hostile Environments on Z" Grand Challenge LDRD project (2014-2016) [11]. A summary of the relevant work exploring ASW appears in Appendix B.

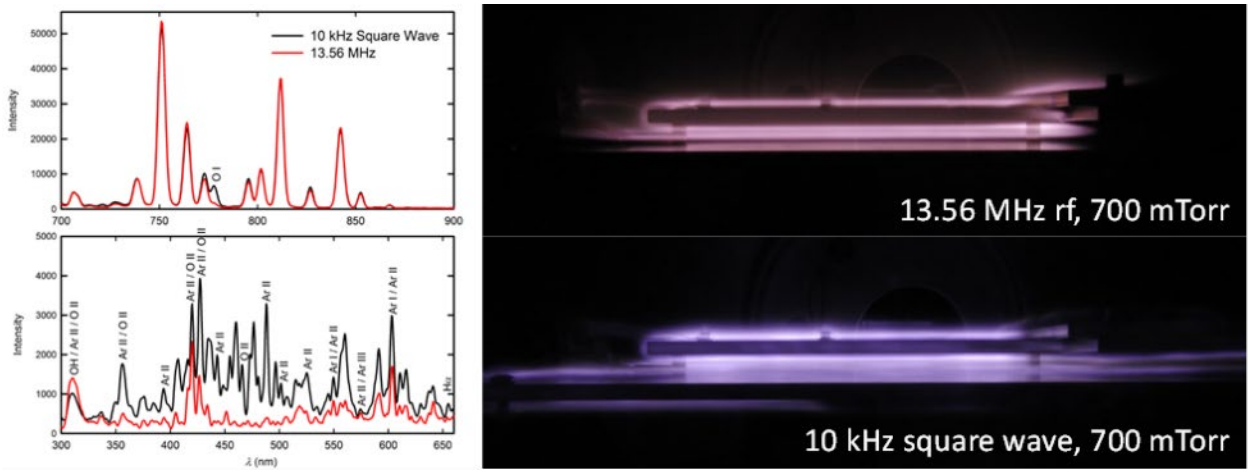

Figure 8: RF (right, top) and ASW square waves (right, bottom) shown in a light-lab testbed during cleaning comparison testing [11]. The ASW plasma achieves higher ionization states, as observed by the bluer glow and higher energy lines in recorded spectra (left)

The ASW high-voltage driver utilizes a positive- and negative-HV power supply connected to a common transmission line via a fast switching pulser. The switcher is driven by a square wave with frequency selectable between 1 and 50kHz, essentially switching between the HV supplies at audio frequencies. The switching voltage is applied to one of the two electrodes in a low impedance accelerator while the other acts as an ASW circuit common. We connect the HV output to the cathode of Z and Mykonos while grounding the anode. This allows the system to leverage the already-grounded anode conductors and reduce the number of insulating breaks.

Insulating breaks are needed to isolate the excitation voltage in the regions with smallest gaps, highest power densities, and largest amounts of parasitic current loss. This prevents the power supplies from shorting out to the anode through geometries of the accelerator. Both Z and Mykonos have water sections that would otherwise short the HV output with a load of a few ohms, which would prevent the supplies from maintaining the needed voltages to ionize the process gas.

3.1. Plasma Cleaning Experimental Platform on a 0.5-MA Accelerator

The purpose of our Mykonos experiments is to evaluate the utility of cleaning for decreasing contaminant plasma formation and reduction of associated parasitic loss processes in low impedance systems. Plasma mitigation through contaminant cleaning has been successful in improving high impedance diode performance in previous work on larger gap (8-12 mm) diodes [6], [7]. However, small gap, high current, low impedance transmission lines are a far more demanding environment with electrodes that are driven to higher temperatures, and for which performance might be sensitive to lower levels of contamination of order a few monolayers (1 monolayer (ML) = 1e15 particles/cm^2). Experiments are needed to determine the utility of cleaning for the more demanding transmission line conditions.

We have designed a Mykonos transmission line experiment that will enable us to directly detect changes in the electrode plasma environments with visible-spectrum diagnostics (cameras), and indirectly infer via electrical diagnostics (current, voltage sensors). The platform design followed from these requirements:

1) The primary experimental MITL ***must*** be diagnostically accessible for both plasma-cleaning and shot-time diagnostics.
2) The experimental MITL ***must*** be the highest electric and magnetic fields in the experiment.
3) The experimental MITL ***must*** generate a current density that is sufficient to raise the electrode temperatures by 400 °C which is required to form plasma from contaminants [3].
4) The load platform ***should*** generate current loss that is resolvable with electrical diagnostics.

Emphasis is added to these objectives to underscore the desire to diagnose change in electrode plasma formation and evolution resulting from a discharge process. There is precedent for Mykonos load platforms to produce observable current loss, like the coaxial MITL experiments of Hutsel ([8], [9]) upon which the *in situ* heating experiment is designed. The Hutsel platform uses ~1 mm AK gaps in a coaxial configuration with a 3mm cathode rod. Our experience with previous glow discharge treatments of high impedance vacuum diodes **(**[6], [7]) and testing with the ASW system questioned whether a cleaning discharge could be generated in a 0.5 – 1.5mm gap. We decided it was too risky to primarily evaluate project success by whether we could observe reduced system current loss following a plasma cleaning process. Instead, our objectives center around observing changes in the electrode plasmas that are hypothesized to contribute to parasitic current loss. The platform we developed provides the diagnostic access to observe these phenomena.

The novel parallel plate design also generates a higher lineal current density than the previously published coaxial geometry ([8], [9]) – and therefore higher electrode heating rates – than the coaxial load platform. Lineal current density is an important figure of merit for accelerators. *Areal* current density is expressed in amperes per unit area; *lineal* current density is expressed in amperes per unit width, or commonly MA/cm. This abstraction is a fundamental way to express transmission line magnetic field strength, i.e. lineal current density $J_l \equiv \frac{\boldsymbol{B}}{\mu_0}\ (\frac{A}{m})$ [12]. This abstraction permits comparison of different accelerators by relating them by the transmission line field strength. A Mykonos experiment can therefore approximate Z conditions at an equivalent inner MITL radius. A higher lineal current density corresponds to higher magnetic field and more rapid ohmic heating of electrode surfaces.

Figure 10 plots a simple calculation of the time it takes to heat stainless steel conductors with a 125 ns risetime current pulse. All current is assumed to flow within one skin depth of the electrode

material. The current distribution is further assumed to not diffuse into the conductor, nor does the conductor experience a temperature-dependent change in specific heat or resistivity. These are fair assumptions for a 400°C perturbation. Steady-state simulations of the Mykonos parallel plate platform suggest the cathode and anode surface areas in the MITL flow are carrying 2.1 MA/cm and 1.8MA/cm respectively. These estimates are subject to the same assumptions described earlier.

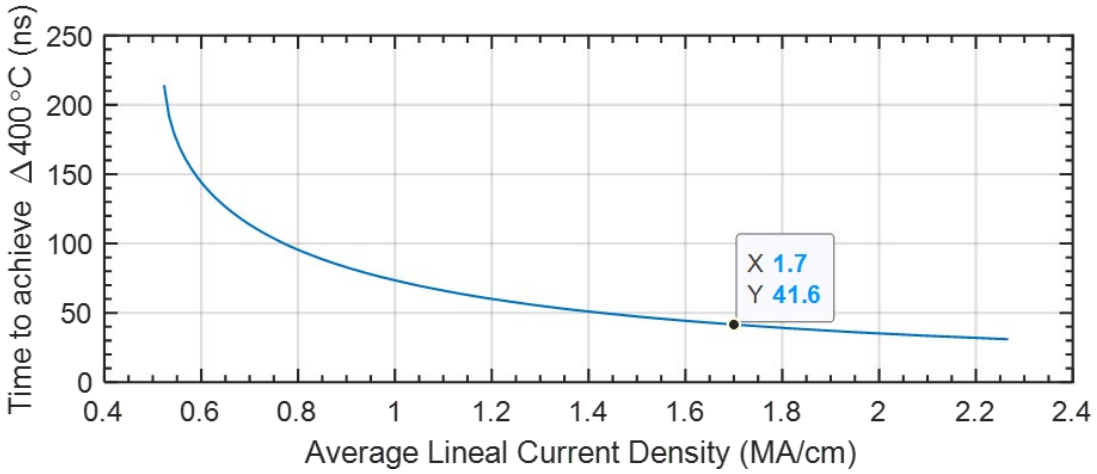

Figure 10: Time required for an electrode to achieve $\Delta T = 400°C$ for 680-kA, 125-ns Mykonos current pulse given a specific lineal current density. A change of 400 °C is known to desorb neutral gases that ionize and form electrode plasma.

The previous figure shows a half-section of the hardware design that meets these criteria. The configuration converts the azimuthally symmetric Mykonos driver into a parallel plate MITL with a

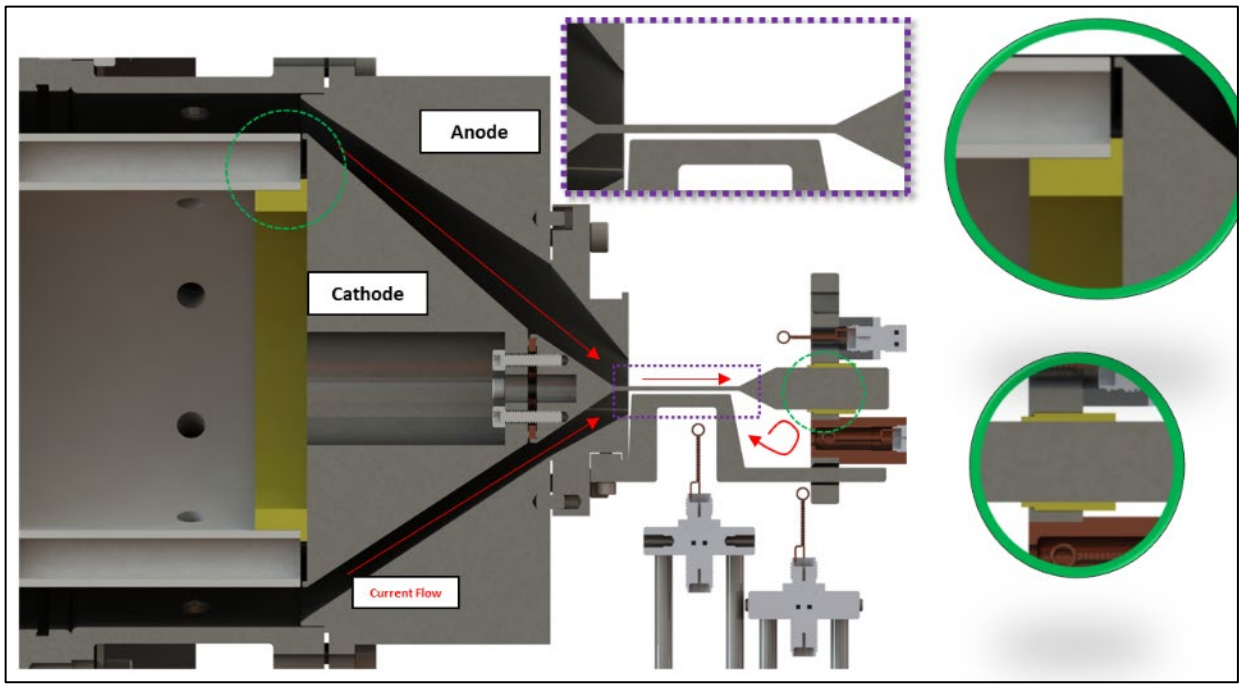

Figure 9: The Mykonos Parallel Plate Platform (MP3) produces a diagnostically accessible high-field region for power flow physical processes to be observed. The anode-cathode gap in the experimental MITL (inset) can be varied between 0.5mm and 2mm while achieving ~2.1 MA/cm lineal current density on the cathode and ~ 1.8 MA/cm on the anode. The cathode has an elliptical cross section (see Figure 30 in Appendix C).

short circuit load. The transmission line uses an elliptical cathode cross-section to produce an approximately uniform current density. Variations of the test MITL cathode and anode pieces permit anode-cathode (AK) gaps between 0.5mm and 3mm and achieve cathode and anode current densities up to 2.1MA/cm and 1.8 MA/cm respectively with a 680-kA current pulse. These estimated lineal current density values exceed that found in the post-hole convolute region of Z (nominally 0.33 MA/cm on the anode post for 20MA) and is equivalent to lineal current density conditions at about 1.6 cm radius in Z's inner MITL. We expect that the electrode heating conditions, and therefore associated contaminant desorption and ionization, will be similar. These conditions are produced for a 2.2-cm long MITL, as shown in the dotted purple inset.

Insulating breaks are highlighted in the green insets of the above figure. These features electrically isolate the cathode from the rest of the experiment during the plasma cleaning process, allowing the transmission line cathode to be the high voltage electrode for the plasma discharge. One of the key aspects of experiments on Mykonos is to evaluate the performance of insulating breaks on the nominal performance of power through the MITL. We have attempted one high power ASW cleaning shot on the Z accelerator (Z2989 in 2016). This shot exhibited poor current delivery for reasons that are not entirely understood, but we believe are related to the presence of insulators in the transmission line regions. These earlier attempts have motivated the more systematic and higher shot rate study described in this report.

A spring-loaded plunger (not shown) contacts the cylindrical feature to the right of the test MITL during the cleaning phase, applying the ASW excitation to the cathode. The insulating breaks concentrate the cleaning plasma in the high-power-density regions bounding the current shown in red arrows in Figure 10. The insulating breaks are designed to produce ~1mm surface distance standoffs that holds off the ~1kV ASW voltage source but present a minor perturbation to the forward traveling ~350kV pulse from Mykonos.

Current sensors (B-dots) are located before (upstream) and after the test MITL to determine if current loss occurred via electrical diagnostics. There are four sensors shown in Figure 11, three free-field loops and a fourth located inside a copper flux excluder directly located in the current flow path. These have been calibrated in offline tests. Further data analysis of these probes is planned but not included in this report. Upstream measurements are provided by standard Mykonos current diagnostics just outside of the experimental region. The figure also highlights the shared field of view of two fast-framing intensified CCD (ICCD) cameras capable of 3-5 ns exposures during the 125-ns current pulse. We have collected the first-ever images of electrode plasma formation with and without plasma cleaning; those results will be discussed in the next section.

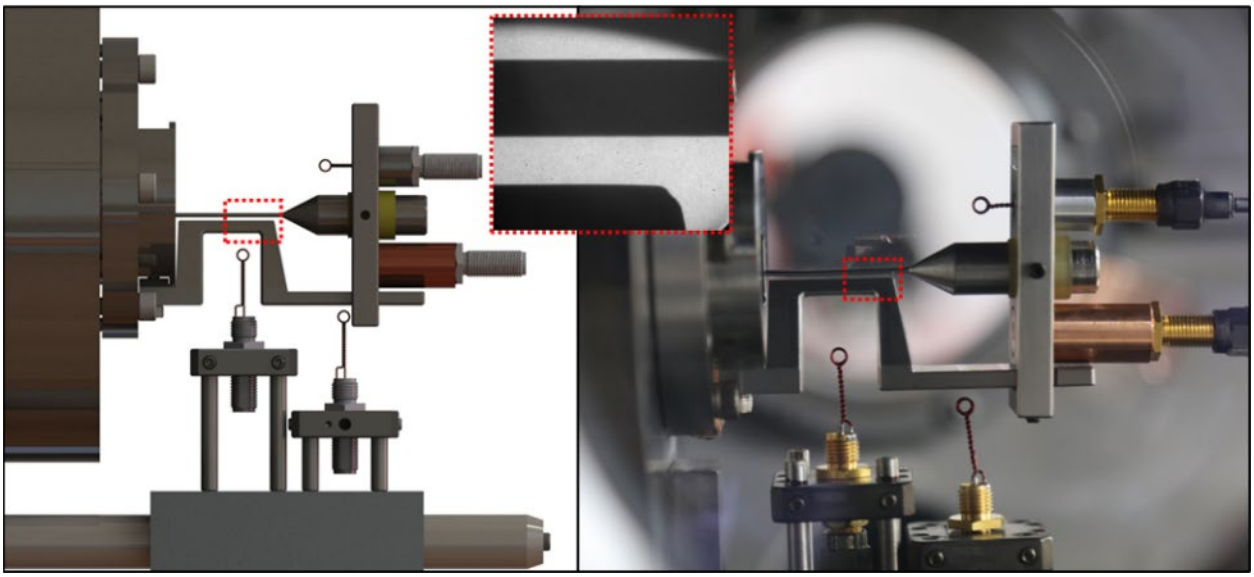

Figure 11: Side-view of a 0.5mm AK spacing, 2.1 MA/cm experiment (model left, as-built right). Inset is the magnfication-4 field of view (backlit), for one ICCD; the cathode and the bend of the anode knee are visible. Power flows to the right in all images. Camera field of view relevant to Figure 16 and Figure 17.

It required several iterations of this hardware to arrive at the configuration discussed in this report. Hardware sets were tested and iterated over three experimental series in FY2021; the lessons learned, insights, and improvements of those tests culminate in the shot series presented here. The plasma cleaning system was integrated into and commissioned at the Mykonos facility in May 2021, enabling this experimental campaign to be performed in July-August 2021. Tests utilizing the 1.8 – 2.1 MA/cm lineal current density cathode with AK gaps between 0.6 – 1.4 mm are presented. These shots were all nominally "0.5 mm gap" configurations, but tolerance issues during assembly caused some variability in each as-built set. The effects of this gap variation are discussed next.

Table 1 provides a tabulation of the relevant experiments and compares shots with and without plasma cleaning. As-measured peak currents, ICCD-image-derived AK electrode spacing, and insulator flashover time are noted. Color coding indicates whether a plasma cleaning process was (green) or was not (pink) employed. All shots had upstream and downstream insulating breaks present. The plasma cleaning protocol was determined in shots prior to Shot 2C15 and maintained constant until shots 2C25 – 2C26, when the cleaning duration was halved from 90 minutes to 45 minutes with all other parameters remaining equal. Shot 2C26 was also 1-mm AK gap spacing hardware because 0.5mm AK gap hardware inventory was exhausted. We note contributions to a systematic AK gap spacing difference between cleaned and uncleaned experiments (1 mm vs 0.8 mm on the average respectively): (i) inexperience in assembly of cleaned experiments early in the series (2C16, 2C18); (ii) tolerance stack-up of the overall load hardware design (throughout), and (iii) remote plunger used to momentarily contact the ASW supply with the cathode (notably 2C16, 2C18). We will work to mitigate these contributions to systematic error for future work. The repeatability of AK spacing for 2C22 – 2C25 (between 0.67 and 0.81mm) is representative of gaps achievable once the installer is experienced with aligning and properly spacing the components.

Table 1: Plasma Cleaning on Mykonos shot matrix figures of merit

Shot name	AK Gap (mm)	Peak Current (MA)	Time of flashover	Plasma process?
2C16	1.39	0.67	178	Yes
2C18	1.21	0.68	175	Yes
2C22	0.67	0.66	183	Yes
2C23	0.77	0.67	181	Yes
2C25	0.80	0.69	178	half
2C26	1.17	0.68	184	half
2C15	0.58	0.70	201	No
2C17	0.71	0.68	201	No
2C19	0.95	0.75	230	No
2C20	0.70	0.68	203	No
2C24	0.81	0.68	201	No

Shots utilizing plasma cleaning used the same cleaning protocol, as follows:

1) The Mykonos load vacuum chamber is pumped down to approximately 1e-04 Torr, which is a pressure that is acceptable for nominal performance of uncleaned transmission lines.
2) An 80% argon, 20 % oxygen (ArO2) gas mixture is introduced with a flow rate sufficient to maintain 900mTorr while the chamber continues to pump at approximately 1.4 L/s. Argon provides physical sputtering of contaminants, while oxygen provides enhanced chemical gettering for contaminants.
3) A plasma is ignited using 75mA excitation current, delivering approximately 25 W.
4) This plasma is sustained for 45 minutes. The chamber is then pumped again to 1e-04 Torr.
5) Gas flow is re-established with an equilibrium chamber pressure of 600mTorr.
6) A plasma is again ignited with 75mA excitation current for 45 minutes.
7) Process gas is turned off, the chamber is pumped down to the required vacuum for nominal performance (1e-04 Torr), and Mykonos is fired as quickly as achievable, typically within sixty seconds. The hi-vac pump is isolated from the chamber just prior to downline.

There were no special cleaning processes used before installation into the Mykonos load chamber. Hardware was unpacked from the vendor, cleaned with isopropyl alcohol, stored at atmosphere, and handled by gloved hands. Low power density pieces upstream of the test MITL are cleaned and refurbished for reuse between shots. Refurbishment was done with alcohol wipes and sandpaper to remove deposited metal slag in regions where the AK gap is of order 8-10mm. No evidence of compromised shot performance has been attributed to refurbishment of these components with the *in situ* discharge cleaning parallel plate platform.

At step 7 when the process gas is turned off, the electrodes may be recontaminated by gas that remains in the vacuum chamber. For example, at a base pressure of 1e-06 Torr, about 1 monolayer of atoms per second collides with the electrodes. We do not know how much of this gas re-adsorbs to the electrodes. An approximately sixty second delay was achievable by coordinating plasma controller operations and Mykonos accelerator charging. During this period as many as 6000

monolayers of chamber gas collides with the electrodes at a pressure of 1e-04 Torr. Electrodes which we believe may have been heated up to 50-100 °C by the discharge power and particle bombardment could minimize sticking and recontamination.

This is another significant uncertainty that motivated tests on Mykonos - will the cleaning process be effective, despite the time it takes to remove the discharge gas, during which the electrodes may be recontaminated? Computational models of power flow indicate that 1-20 monolayers present on electrodes can impact plasma formation and power flow [13], [14], [15]. This is also in the range of inventories that are measured on typical stainless-steel electrodes. Will the discharge process result in a net reduction of surface contaminant inventory, despite the possibility of recontamination?

The intent of our two-stage cleaning process is to generate cleaning plasmas whose spatial extent is efficient at cleaning different regions of the experimental hardware. The 900 mTorr setting creates a visible sheath of the order of the AK gap spacing; it is intended to clean the experimental MITL and the load region. The 600 mTorr is set to clean the upstream components while preventing the load hardware from being recontaminated. Figure 12 shows the characteristic vacuum pressure log and observed discharge plasmas in the load region.

These plasma parameters and cleaning durations were empirically chosen from results of Mykonos shots in FY21; details of these initial experiments are omitted from the scope of this report. We anticipate future work to identify optimum plasma parameters and cleaning durations that minimize

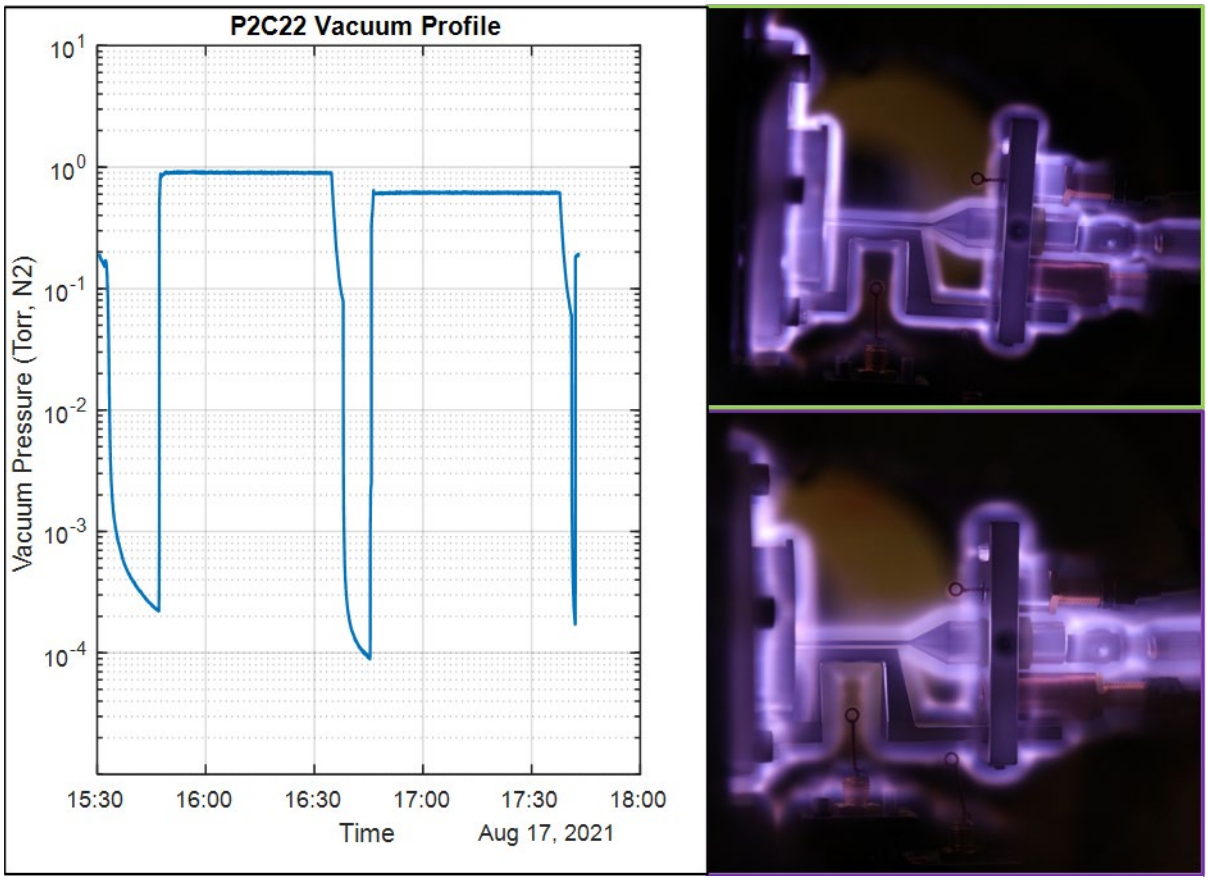

Figure 12: Vacuum chamber pressure log for shot 2C22 showing the two cleaning processes at 900mTorr and 600mTorr (left). The resultant plasma for 900 mTorr (upper right) and 600 mTorr (lower right) present visibly different sheaths.

the time required to clean and therefore to shorten the period for this process in an accelerator shot timeline. Alternate insulator materials such as the ceramic Macor may allow us to increase the cleaning power, increasing the contaminant removal rate, heat the electrode, and extend the acceptable duration before a downline shot. We may also wish to develop methods to provide discharge plasmas at as low a gas pressure as possible, to minimize the pump out delay before reaching an acceptable shot vacuum pressure.

In total, six uncleaned and seven cleaned shots were taken using the experimental platform shown in Figure 11. This grouping of shots had similar enough AK gaps to enlist comparison of shot-time data between otherwise independent experiments. These results are summarized in the next section.

3.2. Results and Discussion of Mykonos Experiments with Plasma Cleaning

The results of these experiments are very encouraging for the utility of plasma cleaning on low impedance pulsed power systems. Electrical data strongly suggests that the late time load impedance is increased by contamination removal, indicating that parasitic current paths have been reduced. For the first time, a plasma cleaning process has been shown to reduce the spatial extent and brightness of self-emission of electrode plasma as observed via the fast-framing ICCD cameras. Although such results have been inferred indirectly in previous experiments [6], this is the first time that these impacts on plasma extent have been directly measured on cleaned electrodes.

The following two figures plot current (I) and the time-rate-of-change of current (I-dot) for the experiments summarized in Table 1 above. We note that shot 2C14 is included in these plots despite being excluded in Table 1. This shot utilized slightly different chamber backfill pressures noted in the previous section (800 mTorr and 500 mTorr for the two stages instead of 900 and 600 respectively). The observed trends were consistent, so the shot was included.

It is challenging to draw strong conclusions from this dataset based on current traces alone. The cleaned shots show a somewhat longer risetime and lower peak consistent with a consistently higher load impedance. Such behavior is requisite to conclude that current loss has been mitigated, but we cannot ignore the systematic trend of a larger AK gap in the cleaned experiments that introduces a 20% larger AK gap on average. This alone could explain a 2-3% decrease in peak current. We note in the previous section that the installer's growing experience with hardware assembly did begin to reduce the variation in AK gap spacing. If we further limit our dataset to AK gaps between 0.67 and 0.81 mm (and exclude 2C25 because of the half-duration cleaning profile), we observe that the trend persists for shots with nearly identical AK gaps. This trend needs to be confirmed with more data than just the five total shots shown here, but initial results are encouraging. These probes are

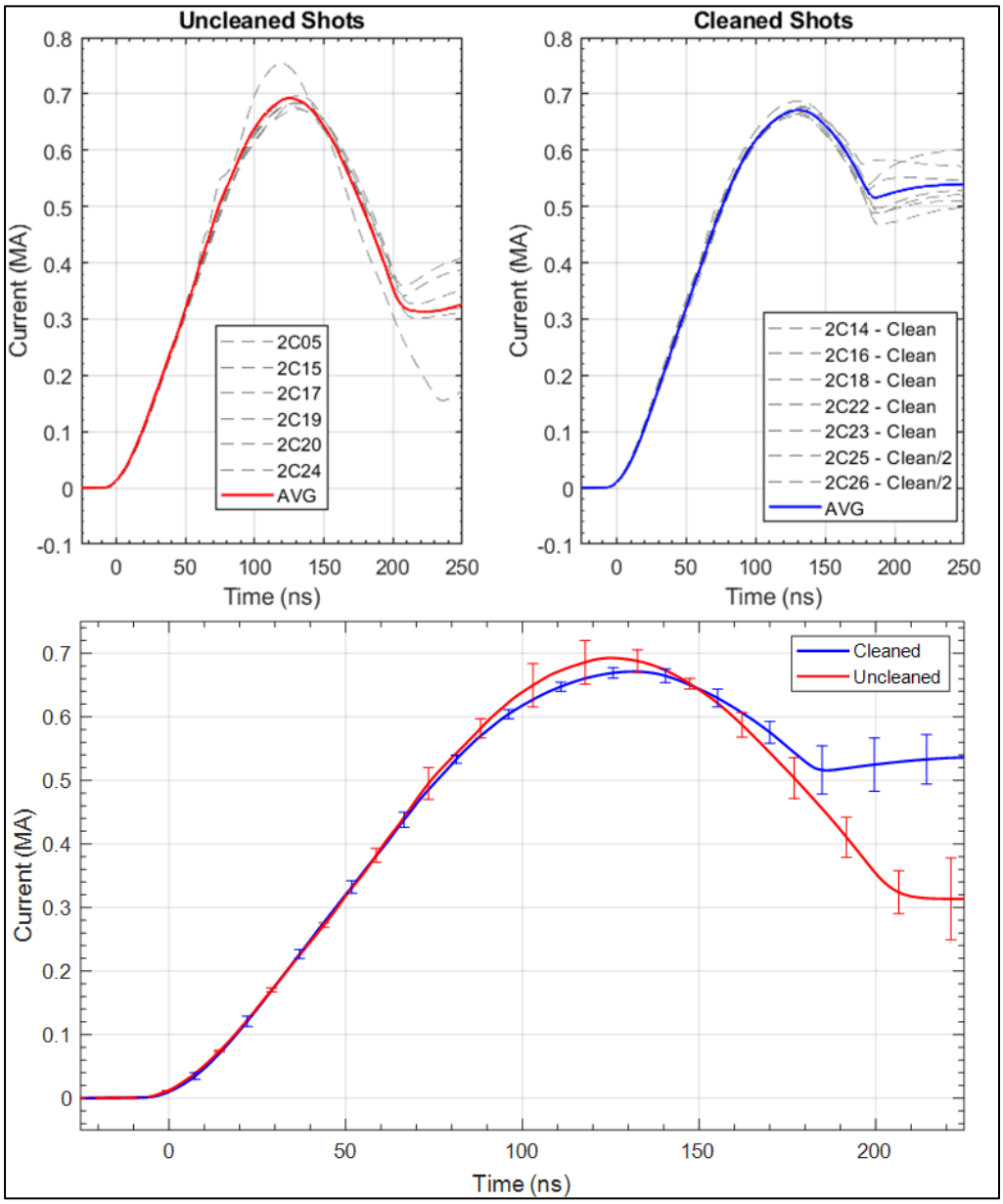

Figure 13: Mykonos delivered current pulses for uncleaned (top left) and cleaned (top right) experiments. Averages are overlaid to show general trend. Average values are also plotted against one another with standard deviations (bottom).

upstream of the experimental MITL. The divergence that begins at 75 ns suggests that the dynamic impedance of the load volume begins to change more for an uncleaned than for cleaned shots.

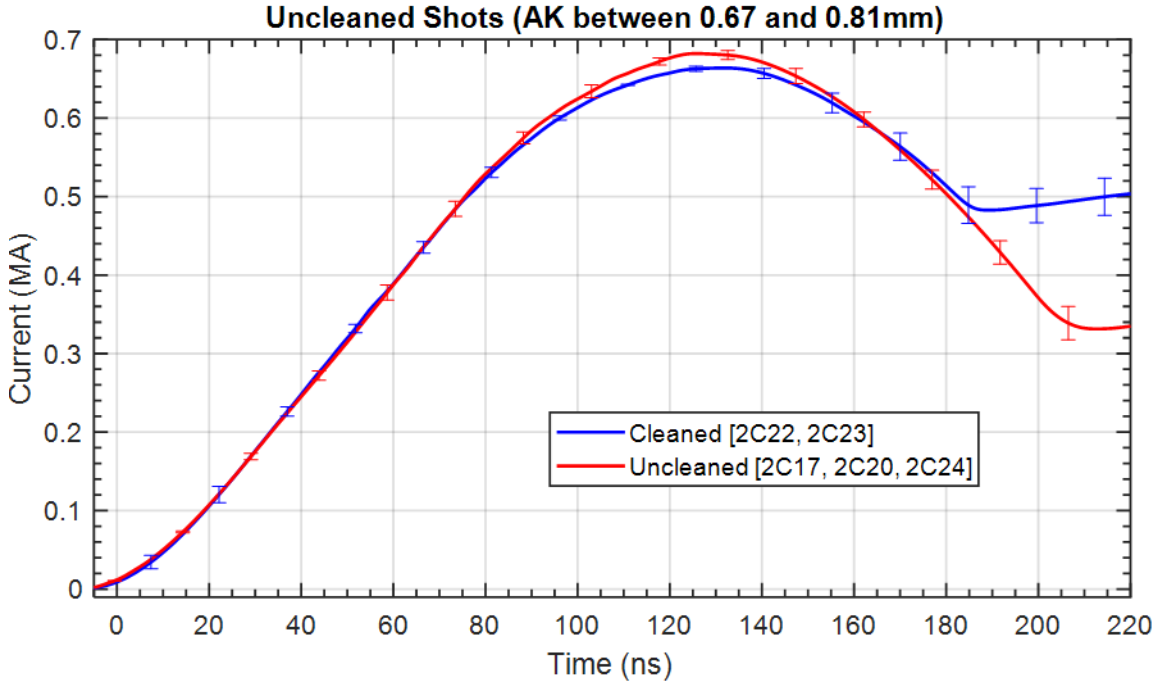

Figure 14: Avg current traces for cleaned, uncleaned shots with AK gaps between 0.67 – 0.81mm.

Particle in Cell (PIC) modeling using the Chicago multi-physics code [16] shows that the parallel plate configuration tends to suppress plasma expansion across the AK gap in the experimental MITL AK region; plasma pressure and magnetic field drifts guide the charged species around the electrodes into the open, lower-field regions. These calculations are discussed in more detail in Appendix C. A primary hypothesis under investigation in the power flow topical area is that gap closure via expanding plasmas contributes to parasitic current loss. We note that while this platform likely will not produce significant current loss observable on electrical diagnostics, it will offer a view of the evolving plasmas, their densities, and an opportunity to characterize the time dependency of these parameters. These observations can be made in the diagnostically accessible region and a more nuanced understanding of the effect of plasma cleaning can be gathered. The ICCD imaging of self-emission electrode plasma discussed later provides the first step towards understanding the effect of discharge cleaning on the dynamic nature of MITL electrode plasma.

Pending analysis of the downstream current monitors will allow direct measurements of the current loss and determinations of the current coupling efficiency for uncleaned and cleaned cases. We predict reduced current loss in the cleaned case consistent with the inference of lower parasitic losses and higher operating impedance for the transmission line.

Figure 15 shows that uncleaned shots have a significantly delayed insulator flashover by about 27 ns, as observed when the positive I-dot signal quickly drops to near zero. The average values for uncleaned flashover are 207 ns compared to 180 ns for the cleaned experiments. This observation indicates that the cleaned hardware is presenting higher late-time impedance to the accelerator well after peak current at about the times that dynamic loads would be imploding on the Z accelerator. This observation suggests that the uncleaned hardware has a more dynamic electrode plasma that leads to late-time parasitic current losses and lowered impedance presented to the transmission line compared to hardware that is cleaned.

The ICCD images relate compelling data about the effect of plasma cleaning. An optical beam line with splitter was designed to provide the same field of view for the two cameras with an overall magnification of 4. This allows two images to be collected per shot of the same spatial feature

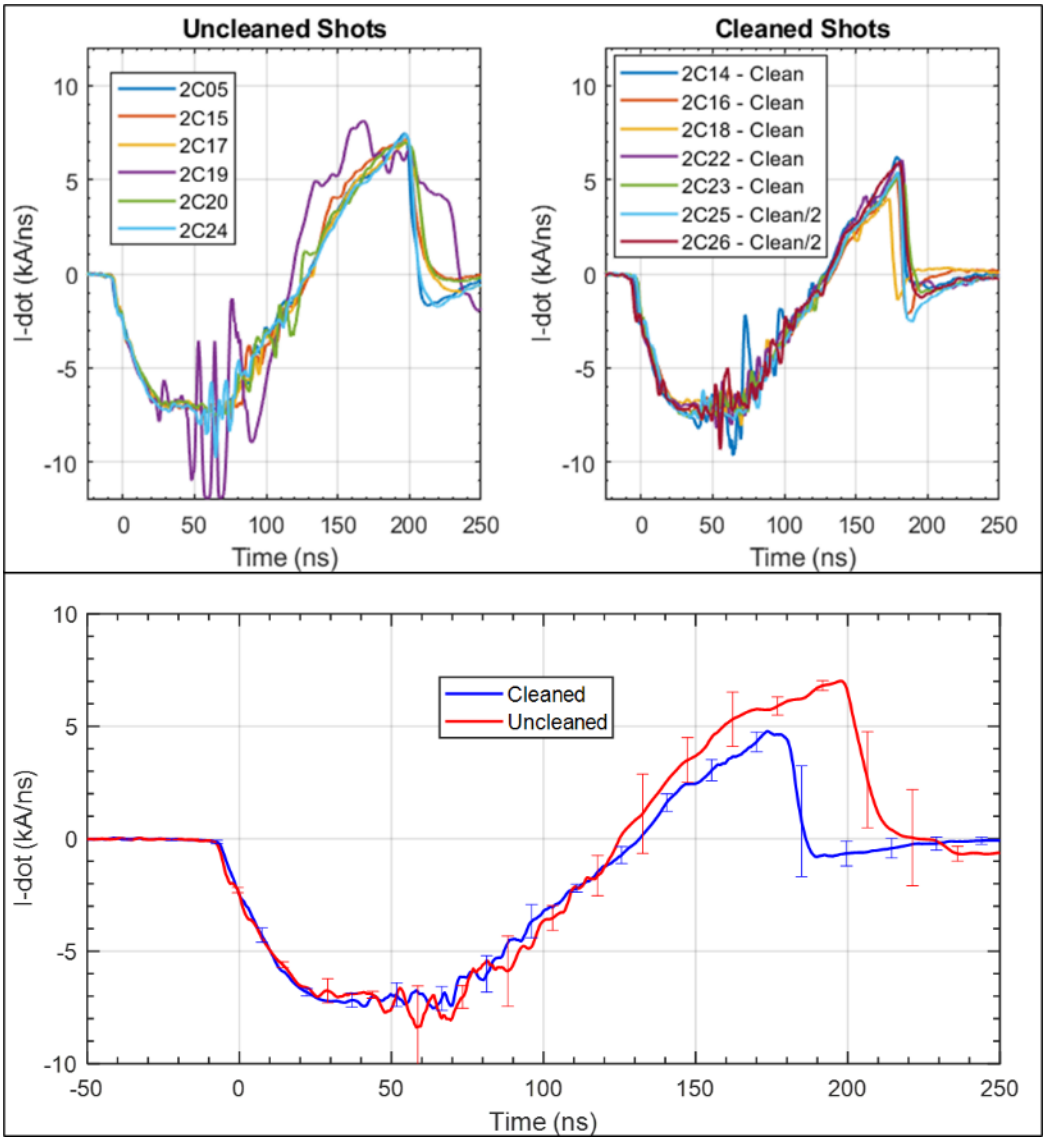

Figure 15: Mykonos upstream negative I-dot signals for uncleaned (left) and cleaned (right) experiments. Insulator flashover occurs approximately 20 ns earlier for the cleaned shots compared to uncleaned. Average values with standard deviations are shown (bottom).

shown earlier in Figure 11, purple inset. Analysis of pre-shot fiducial images show a resolution of 3.4μm per pixel, permitting high resolution images of the ~0.5 – 1.0mm AK gaps.

The two frames targeted approximately 60-70ns and 70-90ns with respect to machine current reaching 50kA. Mykonos trigger jitter of approximately 10 ns contributes to shot-to-shot variation of camera exposure with respect to the current pulse. The following figure shows a series of early-time images for shots with cleaning (top set) and without cleaning (bottom set). Images have been compensated for exposure duration, camera gain, and neutral density filters in the system, and have been plotted on the same intensity scale. The self-emission intensity is dramatically reduced on shots with a plasma cleaning process by a factor of 3 - 5. In these figures, the cathode electrode is on top and the anode is on bottom. A red outline is added to 2C22's image to indicate where the electrodes are located since they are not immediately evident in the image. The anode "knee"

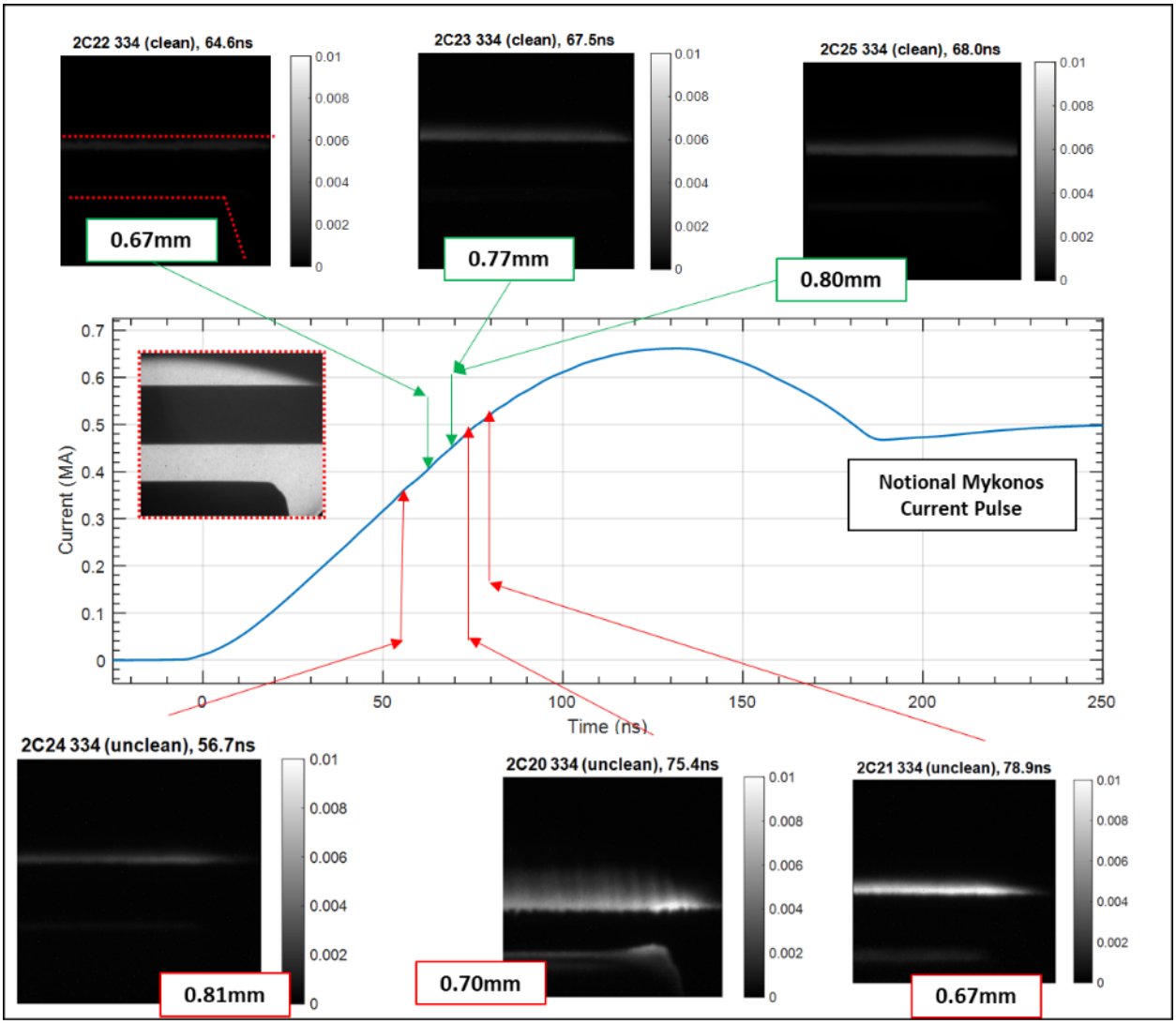

Figure 16: A subset of 3-5ns exposures are shown relative to a representative Mykonos current pulse. All ICCD images are compensated for filters, gain, and exposure and set to the same intensity scale. Cleaned experiments observe a significant reduction in self-emission from electrode plasma.

provides a spatial fiducial that moves in the image depending on alignment, but all images capture the knee feature. Plasmas on this feature is most apparent in 2C20 uncleaned (bottom middle).

Inspection of each figure normalized to maximum intensity shows that plasma emission begins earlier for the uncleaned shots. For example, comparing 2C22 (cleaned) with 2C24 (uncleaned) we observe that the cleaned data, which is acquired somewhat later in the pulse, has minimal cathode plasma emission. In fact, all the cleaned shots (2C22, 2C23, 2C26) at the top of the figure present substantially thinner and less intense cathode plasma emission compared to the uncleaned shots at

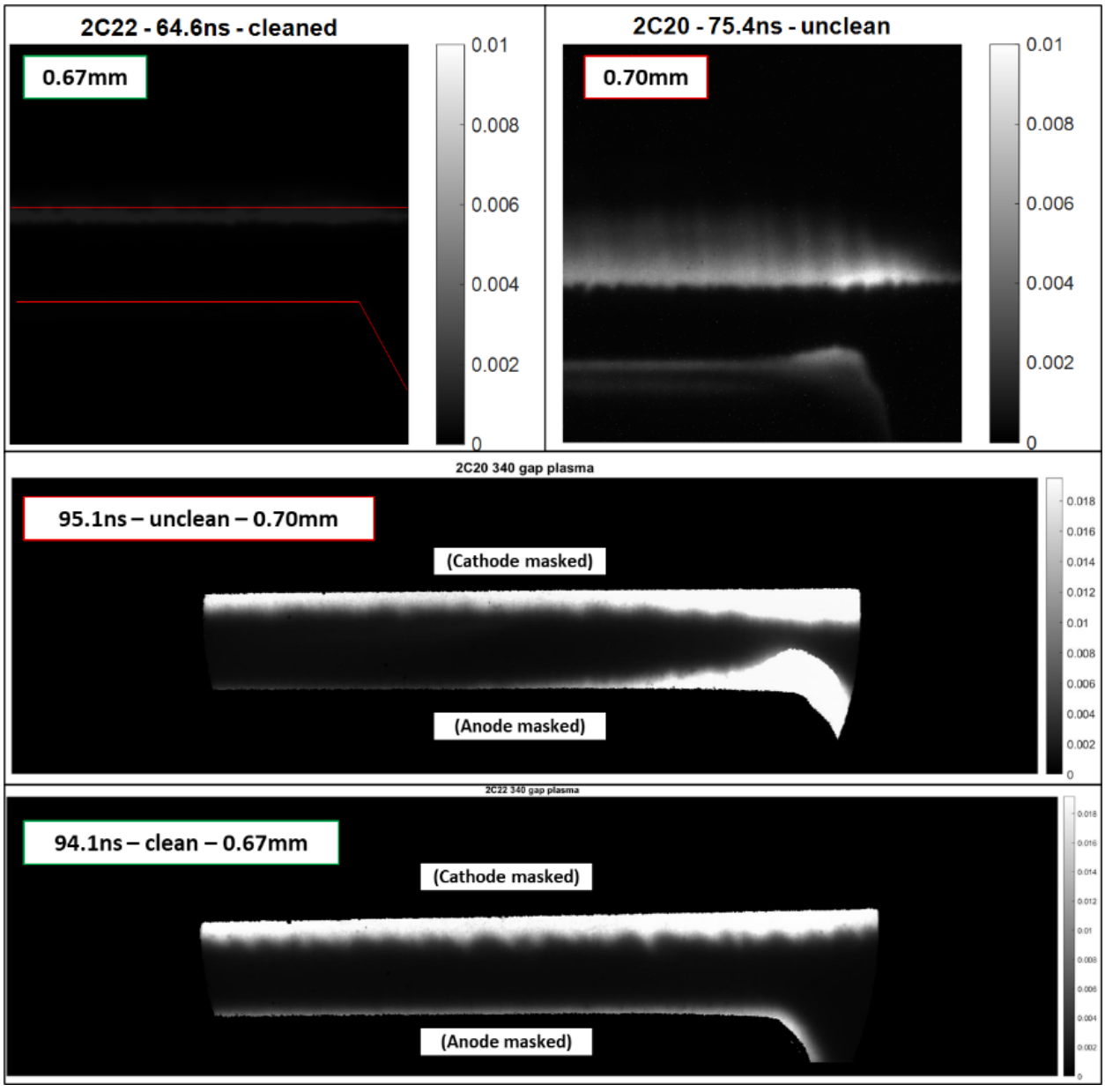

Figure 17: ICCD images of experiments with ~0.7mm AK gaps. Early frames (upper row) for cleaned (2C22) and uncleaned (2C20) show delayed self-emission occurs on hardware with a plasma cleaning process. The inset shows the pre-shot image of the electrodes, with cathode on top and anode on bottom. Late time frames for 2C20 (middle) and 2C22 (bottom) suggest plasma expansion, though significant anode plasma is observed on the uncleaned 2C20.

the bottom of the figure (2C24, 2C20, 2C21). Further still, these images also show suppression of anode plasma, most notably observed in the uncleaned shot 2C20.

We also note the spatial variation in self-emission observed in the cathode plasma along the cathode's length, particularly in 2C20. This variation could indicate the development of an instability in the cathode plasma layer – a fascinating subject for future study.

Figure 17 compares the early- and late-time images from a cleaned shot (2C22) and an uncleaned shot (2C20). These shots were chosen for comparison because of the similarity in measured AK gaps. Though the exposure is 10 ns earlier, the early frame from 2C22 (cleaned) has negligible self-emission (red lines indicate roughly where electrodes are located in the upper left image), while 2C20 has cathode plasma and a growing anode plasma feature. The second frame for these two shots occurs at 95 ns. Both images have had the pre-shot backlit electrode fiducials masked out to highlight self-emitting plasma in the gap. The cathode plasma extent appears to be comparable, though saturation from overexposure in these images limits direct comparison of intensities. Of more interest is the anode plasma on the uncleaned shot which shows that the anode plasma emission front has nearly closed the anode cathode gap at the output end. Anode self-emission intensity of this order is not seen on cleaned shots (2C22).

In summary, an ASW-based plasma cleaning system has been commissioned and demonstrated on the Mykonos LTD accelerator. The conduct of operations for Mykonos experiments was modified to include the additional complexities required for *in situ* plasma cleaning, namely incorporating insulating breaks in the power flow path and modifying chamber pumpdown to accommodate process gas backfill. A cleaning protocol was used on seven shots to compare against a control experiment set of six shots. An *in situ* plasma cleaning process has been demonstrated to have a significant effect on insulator flashover, suggesting electrode plasma formation has been delayed. Fast framing ICCD cameras have captured between 3-5 times lower intensity of electrode plasma self-emission early in the Mykonos pulse. These results are compelling and show that plasma cleaning has a positive impact on power flow, likely through delay of formation and mitigation of electrode plasma expansion. These results also inspire a lot of enthusiasm amongst the team to explore and answer the multitude of follow-up questions, which are noted in the next section.

3.3. Looking Forward: More research on Mykonos, and onward to Z

This initial study of *in situ* plasma discharge cleaning on the Mykonos LTD accelerator has been very promising. We have shown that we can incorporate the required elements to ignite a cleaning plasma and localize it within the highest power density regions, and that these elements themselves do not adversely affect power flow delivery. We have also shown that despite a 60-second delay between removing the discharge gas and firing the machine, the benefit of cleaning persists. The electrical and imaging diagnostics fielded on this experimental series show that *in situ* cleaning delays the formation of electrode plasma and effectively maintains a higher system inductance compared to an uncleaned experiment, indicating a reduction in parasitic current losses. Imaging data suggest delayed plasma formation and expansion, particularly for anode plasma.

This imaging data offers compelling evidence that cleaning electrode contaminants will decrease the plasma density, delay its formation, and reduce its emission. Such data has never been obtained previously. These images cannot yield estimates of plasma density, temperature, or constituent

species, but suggest that they are bright enough to provide emission intensity for follow-on work to characterize these plasma parameters with visible emission spectroscopy during FY22.

Future diagnostics to improve data quality and answer outstanding questions include:

- **12-frame high-speed camera:** Can record twelve, 5-ns frames sequentially or with a 5-ns delay between frames. This will record the dynamics of electrode plasma self-emission over a 60-ns to 120-ns period. Such data will dramatically increase analysis opportunities beyond the two frames of data currently being collected. The entire time evolution of electrode plasma self-emission can be observed for each shot. AK gap closure rates can be calculated for the entire experiment. Growth rates of instabilities can be inferred. The effect of plasma cleaning on all these phenomena can be studied.
- **Streaked Visible Spectroscopy (SVS)**: a streaked visible spectrum can be recorded by an SVS system, allowing time-resolved density and temperature measurements of electrode plasma during and after the current pulse.
- **Avalanche photodiodes**: Time-resolved point measurements of visible or UV emission, can track turn-on time or time-resolved intensity during the current pulse.
- **Novel fiber-coupled interferometer**: Currently in development using Sandia LDRD funding, it should provide time resolved, chordal densities down to approximately 1e14 cm^{-3}.

Diagnostics will also be added to observe the cleaning phase of the experiment:

- **Residual Gas Analyzer (RGA) sampler**: gas will be sampled from the exhausted process gas and fed to an RGA to observe constituent gases generated during cleaning. Active monitoring of reactant productions like OH, CO, CO_2, and H_2O will allow an assessment of how long cleaning must occur before contamination is reduced to reasonable levels. Rates of removal can be inferred, and a cleaning protocol can be optimized.
- **Fiber coupled benchtop spectrometers**: Three StellarNet BLUE-Wave spectrometers will simultaneously cover UV, Visible, and Near-IR emission from the *in situ* cleaning plasma in the experimental region. Plasma temperatures and densities will be determined and correlated to observed cleaning rates from the RGA to further define an optimum cleaning protocol.
- **Offline testing in light-lab facility**: Demonstration of these diagnostics in canonical geometries in an offline facility is paramount to help inform desired observables in Mykonos. A plasma cleaning testbed has been created that permits these same diagnostics to be fielded on a plasma generated between cylindrical faces, parallel plates, and eventually a surrogate buildup of the Mykonos experimental hardware. Testing in this chamber will begin in Q1 FY22.

Much can still be done with experiments on the Mykonos accelerator utilizing plasma cleaning processes. We are planning 12 weeks of facility time in FY22 to support continued experiments. During these shot series, we will explore the following which are pertinent to scaling this protocol to the Z accelerator:

- Establish the fidelity of downstream current monitors and upstream accelerator voltage monitors.
- Incorporate thermocouple measurements that evaluate shot-time temperatures of electrodes following plasma cleaning processes.

- Implement diagnostics summarized earlier to understand electrode plasma formation, densities, temperatures, and observed gap closure in the experimental MITL during Mykonos shot.
- Field optical and mass spectroscopy diagnostics to understand cleaning rates as a function of clean plasma parameters like density, temperature, and system input power.
- Develop a methodology, or possibly new hardware load design to achieve repeatable AK spacing
- Understand effect of neutral desorption from insulating breaks and demonstrate that offline preconditioning (bake-out) or demonstrate ceramic insulators can enable higher power cleaning protocols, or methods that scale to Z
- Explore different process gas species beyond Ar/O_2, e.g. H_2, with different discharge excitation techniques, e.g. RF. Determine effect of staged cleaning protocols (e.g. ASW with Ar/O_2, then RF with H_2) on cleaning efficiency and power delivery. Can H2 discharges be used to remove surface oxides from the stainless?
- Characterize discharge performance with the delay between terminating the discharge and the Mykonos downline pulse – can the effect of cleaning be undone by recontamination? Longer pump out delays are likely required for the Z environment due to smaller pumping speeds, perhaps up to 10 minutes. What is the maximum pump-out delay that still allows an impact of discharge cleaning?

The ASW plasma cleaning technology was originally prototyped for the Z accelerator in 2016 by the Hostile Environments Grand Challenge LDRD. Much of the design work and Conduct of Operations (ConOps) planning was performed during that project, so there are few unknowns or uncertainties in the engineering implementation and integration into an Z experiment. Figure 18 shows the designed load hardware modifications to generate a cleaning plasma in the Z convolute and inner MITL, where most current loss is known to occur. The "Showerhead" is mounted on an electrical actuator to make contact during cleaning but disconnect prior the Z downline shot. The showerhead also contains twelve nozzles that direct gas into the convolute and provide continuous flow to convect reactant products out from the plasma region. Insulating breaks just upstream and downstream of the convolute isolate the ASW excitation to the inner MITL and post-hole regions where loss occurs without risking damage to the target.

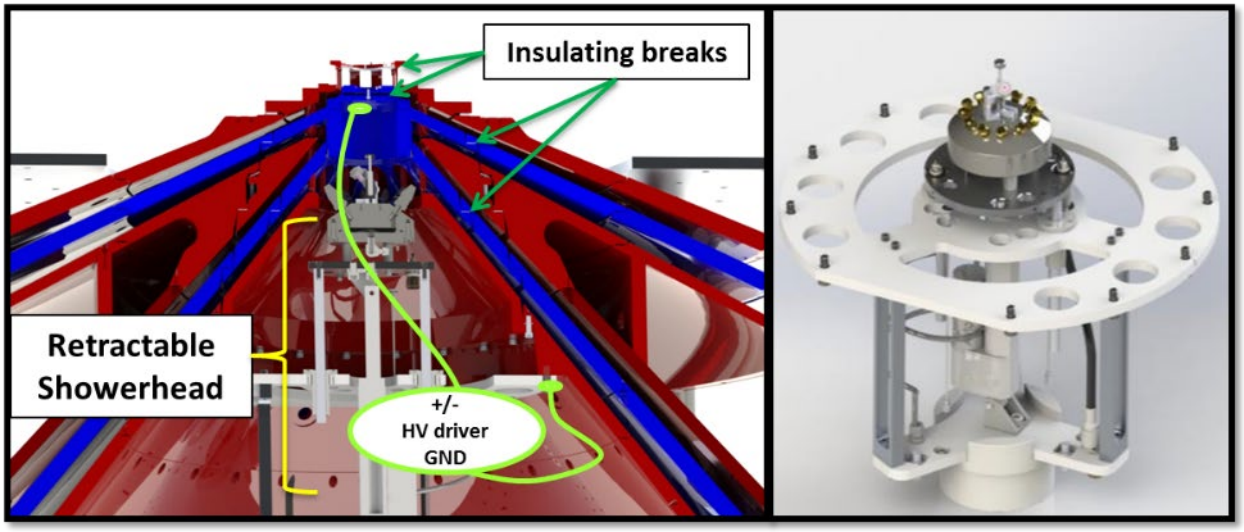

Figure 18: The Z Machine convolute with cathode (blue) and anode (red) conductors shown, with the showerhead installed (left). Insulating breaks are installed to isolate the target and the outer MITLs from the cleaning plasma. The showerhead (right) contains an actuator and gas nozzles to provide process gas flow through the convolute region during cleaning.

The ASW plasma cleaning process was fielded at full scale on a Z downline shot in 2016, with poor results. We believe the plastic insulating breaks contacting the adjacent electrodes heated to ~100 °C by the discharge process, likely introduced neutral gas species that affected power delivery. Experiments on Mykonos during the series described in this report found that ASW discharges at high power melt the plastic insulators on Mykonos and provides credence to this hypothesis. Insulators needed for ASW discharges remain a large risk for high current density experiments on Z. Other approaches to eliminate insulators may be possible, including ceramic pieces or baked out, high-melting-temperature engineered plastics. On the ASW-enabled Z experiment, we needed approximately eight minutes to pump Z from 0.7 Torr discharge pressures to the required vacuum pressure for a Z downline shot. We will study the impact of longer post cleaning delays on Mykonos and explore decreasing the delay on Z through increased pumping, decreased discharge pressure, and possibly firing Z at higher pressures. The exploration we're doing in the light lab and at Mykonos are the first steps to understand how to optimize a cleaning process for a low impedance accelerator like Z. The exact cleaning protocol we develop for Mykonos may not simply map to Z, but the method for designing and evaluating the protocol will.

This page left blank

4. *IN SITU* HEATING

There is a long history supporting the investigation of contaminant removal using *in situ* heating under high vacuum to clean scientific vacuum surfaces and bulk materials dating as far back as the 1960's [17]. More recently, standardized procedures have been defined for surface and bulk material preparation for vacuum vessels and their related hardware. For 300 series stainless steel, it is well known that reversibly chemisorbed compounds for water, carbon dioxide, and other hydrocarbons can be readily removed from a surface at vacuum bakeout temperatures as low as 300 °C; and, that hydrogen can be removed from the bulk at temperatures ranging from 350 – 950 °C [18]. These outgassing species correspond to the chemical reaction of weakly bound surface compounds such as hydroxyls (-OH), carbonyls (C=O), and surface oxide reduction due to hydrogen diffusion. Granted, much of the above work relates to reducing outgassing, diffusion, and permeation for improving the base pressure of large vacuum systems or preventing contamination during vacuum processes; but, the concept is the same – apply heat while under high vacuum to remove surface and bulk contaminants. Appendix A provides more discussion of the theory of contaminant inventories.

In this section, we briefly review the technical background related to our *in situ* heating approach, provide an overview of the experimental platform and summarize our results. We follow with a brief discussion of our findings and lessons learned, then provide a path forward for future research.

4.1. Experimental Platform

The *in situ* heated electrode assembly used in these experiments is based on the high lineal current density coaxial platform previously developed by Hutsel et al. discussed in Section 2, which studied the parasitic losses due to vacuum pressure, time under vacuum, and vacuum storage protocols on a 1 mm AK MITL shown in Figure 5 [9]. This previous work observed a correlation between improved power-flow for lower base vacuum pressures, which are believed to correspond to cleaner electrode surfaces. Also, the authors demonstrated that standard hydrogen firing and high temperature vacuum bakeout of the hardware improved power flow provided the hardware was stored under vacuum until just before shot time.

Based on these initial findings, we modified the load hardware design from Ref. [9] to allow for independent heating of the anode and cathode. With this approach, a direct comparison between the two configurations could be made to determine the efficacy of *in situ* heating while simultaneously assessing the engineering challenges associated with integrating high temperature devices into vacuum-based pulsed power. During a two-year LDRD conducted during FY19 & FY20 [19], an initial *in situ* heating concept was developed based on thermal simulations to investigate heating methods for the anode and cathode, and to explore thermal management methods to protect the diagnostics and accelerator components. A conceptual view of the modifications to incorporate high temperature (~500 °C) heating in the coaxial region is depicted in Figure 19. This design leveraged the use of commercial off the shelf (COTS) cartridge heaters located at the top and bottom of the cathode and a brazeable wire heater around the neck of the anode. Though these components are not specifically designed for vacuum use, previous studies demonstrated these heaters can operate above 500 °C while under vacuum without any adverse effects. The initial thermal simulations of the conceptual design are shown in Figure 19.

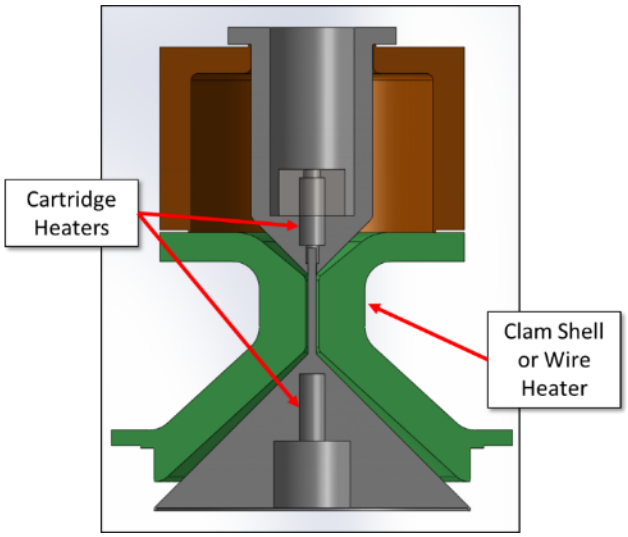

Figure 19: Simplified 3D CAD model indicating locations of cartridge heaters in the upstream and downstream portions of the cathode (grey) and the location of a wire heater on the outside of the anode (green). Note: this view is rotated 90° to machine axis.

In a thermal system such as this, care must be taken to consider proper thermal management, isolation, and mitigation. Due to the low thermal conductivity of steel, several design iterations and simulations were required to arrive at a viable design. Specifically, this system required the use of internal cooling channels to properly isolate the "hot" regions from the rest of the system (e.g. the Rexolite water-vacuum insulator) and to protect the downstream B-dot diagnostics (see Figure 21). To achieve this, we leveraged Additive Manufacturing (AM) to 3D print and then machine the anode and "current return can" using 304L stainless steel (depicted in "green" and "orange" respectively in Figure 19). To the authors' knowledge, this represents the first additively manufactured (AM) hardware to be fielded on a low impedance accelerator. The configuration for a heated cathode experiment is depicted in Figure 21, which highlights the 3D printed "current return can" with two internal cooling jackets within a gyroid lattice.

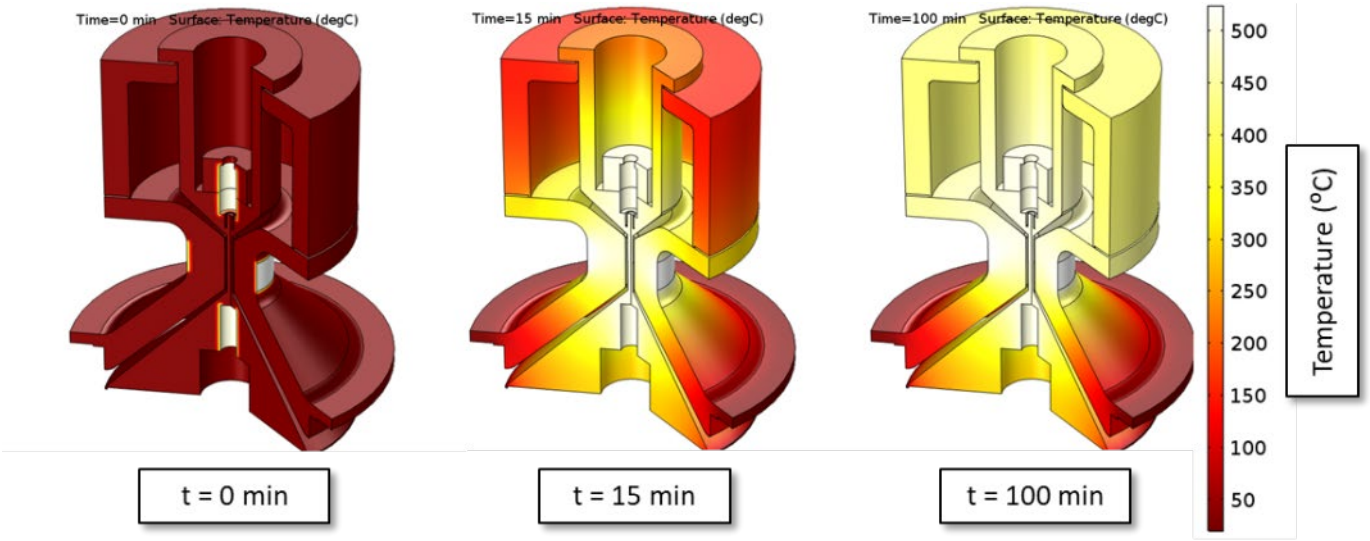

Figure 20: Initial thermal simulations of a simplified geometry with ~500 ºC applied at proposed locations for heaters (shown in 'white' at t = 0 min).

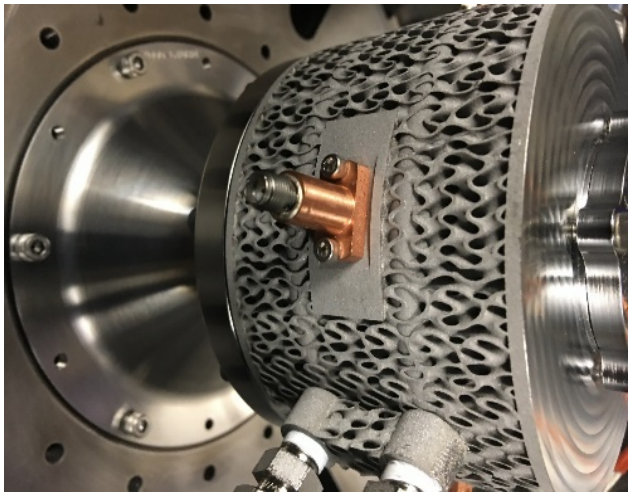

Figure 21: Hardware for heated cathode experiments where the Current Return Can is AM printed in 304L Stainless Steel with internal cooling channels on either side of the downstream SMA connectorized B-Dot.

The following outlines the typical shot procedure for all *in situ* heated experiments:

1) All components were degreased and cleaned using ethyl alcohol prior to installation.
2) Concentricity of the cathode to anode is established via a custom feeler gauge downstream of the coaxial region ("orange" circle in Figure 23).
3) The vacuum chamber was pumped down to approximately 3e-05 Torr.
4) Heating was initiated until the target temperature was reached.
5) Heating continued until the base pressure returned to ~3e-05 Torr.
6) The heaters were disconnected ~10 seconds prior to firing Mykonos.

4.2. Results and Discussion

Initial experiments using the *in situ* heated anodes and cathodes were conducted near the end of the FY20 LDRD campaign. In total, 9 shots were executed: (3x) to validate additively manufactured components perform comparably to conventional hardware without heating, (3x) heating the anode only, (2x) heating the cathode only, and (1x) heating both the anode and cathode. For these initial shots, it appeared the baseline shots for AM components experienced an amount of current loss consistent with the trends established for conventionally machined hardware. However, the six heated shots experienced widely varying amounts of current loss ranging from 12 kA to 380 kA which are summarized in Table 2. It is believed this extreme variability in current losses is a result of (i) warping or deformation of heated hardware since the thermally induced stresses possibly exceeded the plastic deformation limits, (ii) a reduction in the upstream AK gap due to thermal expansion of the cathode, or (iii) misalignment of the load hardware and/or Mykonos mounting plates.

Based on these cursory and limited results, we planned several additional activities in FY21 to better assess the viability of *in situ* heating for improving power flow and to further investigate the engineering challenges associated with fielding high temperature *in situ* heating. These activities included:

1. Repeat heated anode and cathode experiments using spring loaded mounting to reduce thermally induced stresses and mitigate warping.
2. Completing a detailed analysis of Mykonos alignment and hardware fabrication errors and investigate improved alignment techniques.
3. Improving PIC simulations by: (i) incorporating an accurate circuit model for Mykonos, (ii) updating the desorption boundary conditions that incorporate more recent materials measurements (i.e. inventories and binding energies), and as a stretch goal (iii) modeling a shorted AK gap.

It must be noted that progress was impacted due to COVID related closures and delays in the supply chain and manufacturing of new hardware. However, there were still several lessons learned relating to the planned activities above and in support of this milestone as summarized below.

Table 2: Summary of in situ heated shots from FY20 and 21. Data from shots used for troubleshooting or where the load shorted upstream of the coaxial region are not presented.

Shot #	Description	Temperature (°C)	Estimated Loss (A)	AM Anode	Refurbished
FY 2020					
10396	Baseline	~24	66,091	Y	N
10489	Baseline	~24	172,684	Y	N
10491	Baseline	~24	73,819	Y	N
10883	Heated Cathode	560	204,574	N	N
10885	Heated Cathode	560	226,302	N	N
10888	Heated Anode	525	344,572	Y	N
10890	Heated Anode	320	12,266	Y	N
10892	Heated Anode	220	106,357	Y	N
10894	Heated A & K	293, 590	378,323	Y	N
FY 2021					
11127	Baseline	~24	54,000	Y	Y
11129	Heated Anode	320	25,000	Y	N
Mykonos Maintenance and Software Modification (New Shot Numbers)					
10811	Baseline	~24	180,000	Y	Y
10819	Heated Anode	320	341,000	Y	Y
10835	Heated Anode	320	100,000	Y	Y
10868	Heated Cathode	320	200,000	N	N

4.2.1. Lessons Learned

Alignment:

A shot series was executed to fully characterize Mykonos and inspect all hardware based on several high current loss shots, identification of hardware outside of specification (i.e. bent cathode tip with >500 μm error), concerns about the concentricity and angular alignment of the Mykonos load chamber, and the PIC simulation of a misaligned AK gap. These concerns were explored in addition to separate exploration of misalignment caused by to the concerns about misalignment caused by thermal expansion and warping. The results of this study are summarized below.

Using Mykonos as a surrogate test bed necessitates the inherently small (1 mm) AK gap required to reduce load inductance while electrically stressing the MITL. We produce lineal current densities approximately equivalent to the inner MITL on Z with a 3mm diameter cathode rod. These small geometries require precision in hardware design intent and assembly; small alignment errors or translational offset of 200 μm in a 1-mm AK gap will have a large impact on the apparent current loss. Previous studies indicate a peak loss current scaled approximately from 20 kA, to 100 kA, to 400 kA for a 1, 0.8, and 0.6 mm AK gap respectively after a 2 hour vacuum pump down [9]. This suggests an alignment tolerance that requires no more than 100 μm of error along the 4 cm long coaxial region (see Figure 23) of the load where the lineal current density is the highest. Since the downstream concentricity of the hardware can be adjusted during installation, only the angular error between components needs to be established in advance and aligned to within 2.5 mrad.

A dial indicator mounted to a dual pillow block bearing assembly riding along a precision rod were used to characterize the parallelism and concentricity of the anode and cathode mounting plates while at atmosphere. Using this apparatus, the cathode and anode plates (shown as 2 and 3 in Figure 22) were characterized individually on an optical table to determine their flatness with respect to their mounting surface. The cathode plate had an angular error of 1 mrad and the anode plate had an error of 2.2 mrad. Depending on the clocking of the two plates relative to each other, the angular error between the two could range from 1.2 – 3.2 mrad. After aligning the axis of the "Main Cathode Body" to the mating surface for the "Anode Mounting Plate," the cathode and anode mounting plates could be clocked relative to each other to reduce the angular error to 2 mrad. Using the previous alignment techniques, the concentricity was established to within 150 μm.

These initial results were improved by inserting a length of Spira-Shield gasket along the circumference between the Main Cathode Body and the Cathode Mounting Plate (1 and 2 in Figure 22). This allowed for fine adjustment to the pointing angle of the cathode mounting plate. As a quick demonstration, the anode and cathode mounting plates were aligned parallel to within 0.4 mrad while achieving a concentricity better than 0.025 mm. The chamber was then placed under rough vacuum and brought back up to atmosphere resulting in an angular error of 1.1 mrad. This is a result of the Main Cathode Body shifting during pump down since it is secured only by a plastic bolt and an o-ring seal.

Even though these alignment errors may seem unique to Mykonos due to its inherently small geometry, these issues will need to be addressed when scaling to larger accelerators.

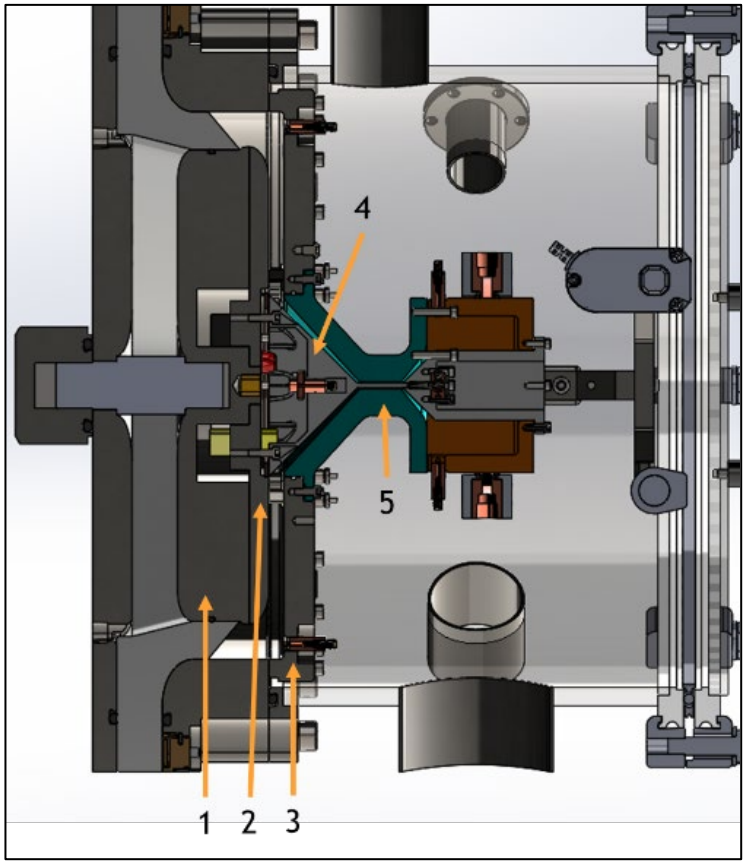

Figure 22: Identification of components requiring critical alignment. 1. Main Cathode Body, 2. Cathode mounting plate, 3. Anode mounting plate, 4. Lower Cathode, 5. Anode.

In addition to the alignment errors inherent with the Mykonos system, we discovered nonconformities of new hardware where the thin cylindrical region (in red in Figure 23) was slightly bent during the shipping process resulting in an ~500 μm error. This bend results in an offset of order 3 human hairs observed at the end of the 4 cm long cathode rod. With the anode in place, this constitutes an azimuthally preferential 50% gap closure in a 1-mm AK gap MITL which would result in undesired current losses. To estimate the impact of such a misalignment, a PIC simulation with using an axisymmetric 500-μm AK gap was conducted in CHICAGO. The general description of how the simulation is configured is described in Appendix D. The upstream and downstream currents are plotted for a high loss shot

(#10888) and PIC simulations shown in Figure 24. This comparison suggests that even a small misalignment could account for current losses of 300 kA and seems to be in reasonable agreement with ~400 kA of loss for a 0.6 mm AK gap as measured in Ref. [9].

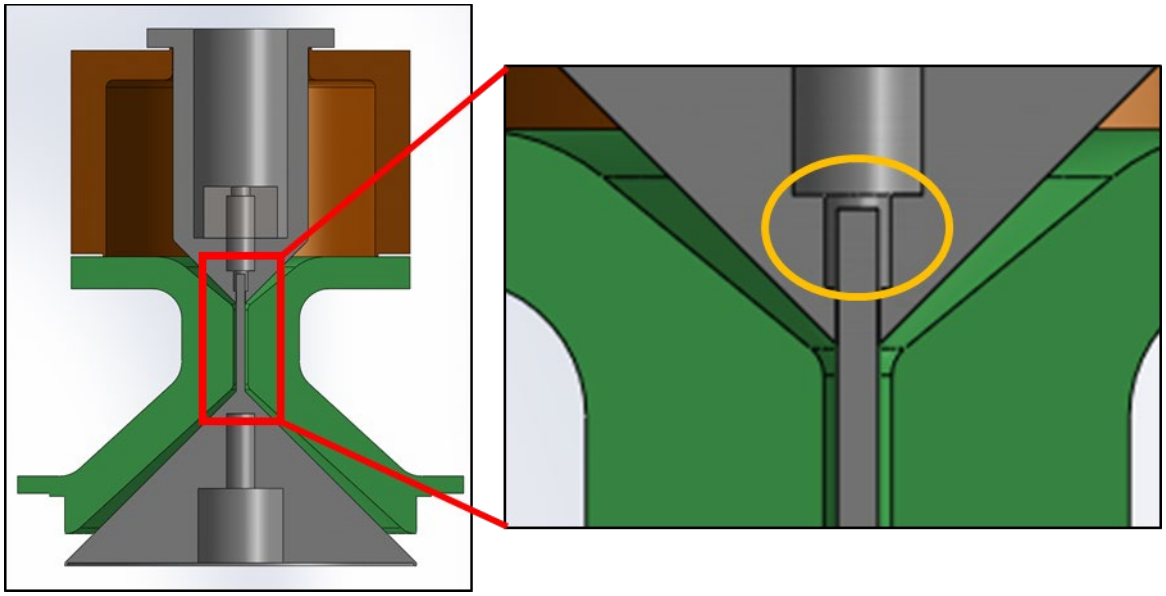

Figure 23: Encircled region of the lower cathode in "red" prone to misalignment due to bending during packaging and transport (left). Zoomed region highlighting portion of cathode which was deflected as much as 500 μm due to manufacturing/shipping errors (right).

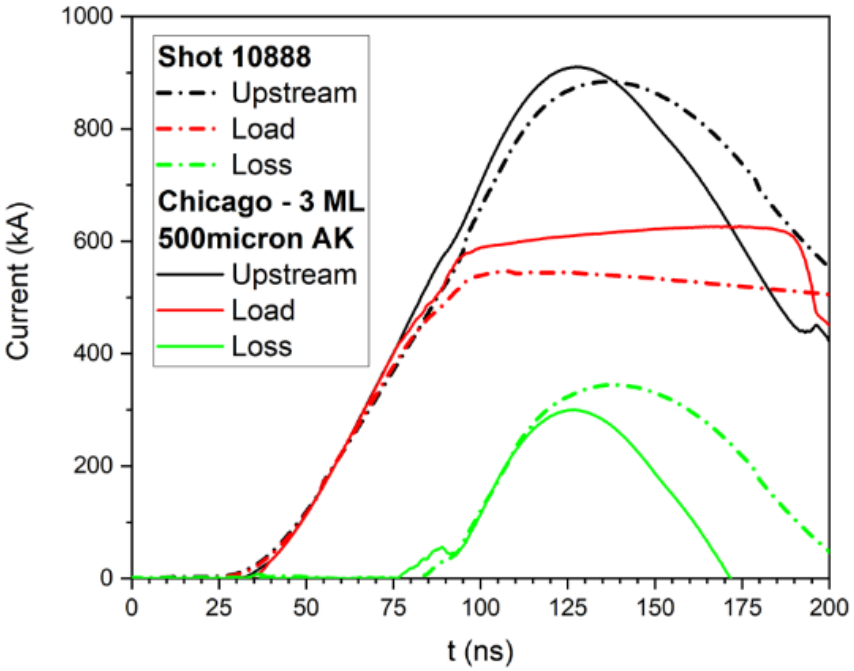

Figure 24: Comparison of 500-μm AK gap PIC simulation to an abnormally high current loss shot in which the coaxial region alignment was suspect. Upstream (black) and downstream currents (red), and their difference (green) are plotted showing a peak loss of 300 – 350 kA.

4.3. Future Experiments and Scaling to Z

This initial study of *in situ* heating of a high lineal current density MITL has been informative. We have successfully modified the hardware to allow for baking out the high current density regions of the load hardware to temperatures exceeding 450 °C without negatively impacting the Mykonos accelerator or other infrastructure. However, large variability in recent experiments, characterization of misalignments, and informative simulations assert that there are several engineering issues which need to be addressed. We intended to perform additional experiments in FY21, but delivery of hardware with improved concentricity and alignment features was delayed due to COVID-related issues with suppliers and vendors. As such, there are several experiments or modifications which would be beneficial to help further understand the loss mechanisms the *in situ* heating modification of the Hutsel platform, help improve the simulations, and provide insight for scaling a heating system to a larger accelerator like Z.

- Experiments on Mykonos require the ability to characterize the alignment of the anode to cathode while under vacuum and at temperature. Even if the alignment of the hardware could be established with high accuracy during install, simply pumping down the vacuum system can result in large errors. Thermal expansion may lead to stresses and unexpected warping that should be quantified prior to shooting.
- Using an alternate geometry, such as the parallel plate MITL from the plasma discharge experiments, could allow for an optically accessible AK gap allowing for real time monitoring of the alignment. This system may be more amenable to high temperature heating without inducing large internal stresses.
- A more comprehensive study of heated cathodes should be conducted to assess the efficacy on reducing current loss. This would help corroborate the results of the plasma cleaning experiments, provide direct comparisons to our existing PIC simulations, and would inform simulation improvements.

This page left blank

5. SUMMARY AND FUTURE WORK

This report summarizes our work in satisfaction of the objectives of the L2 milestone, "Assessment of electrode contamination mitigation at 0.5 MA scale." We presented our designs for a planar *in situ* discharge cleaning and cylindrical *in situ* heating Mykonos load platforms and described our initial findings at the time of this report.

These results show encouraging progress to address requirements for cleaning systems at Z that reduce contamination via an *in situ* removal process. For the first time, the efficacy of such a system will be informed by experimental data on a low impedance accelerator that accesses the same lineal current densities as Z's convolute and inner MITL regions. The coming year will see progress continuing at an accelerated pace to advance the understanding of these process, particularly with the *in situ* plasma cleaning system.

We have completed the grading and exit criterion for MRT 7291 "Assessment of electrode contamination mitigation at 0.5 MA":

> (1) Evaluate both heating and discharge cleaning system engineering designs;
> (2) Evaluate the potential impact on system operation;
> (3) If these systems are viable, evaluate the impact of these systems on several performance metrics including electrode plasma formation and current loss, and power flow at 0.5 MA scale, or
> (4) describe modifications to the designs needed to make these systems viable.
>
> **Exit criterion**: Submit a technical report describing the engineering performance, impact on operations, and potential or actual impact of both heating and discharge cleaning on relevant performance metrics on the Mykonos accelerator

The *in situ* heating system will require further engineering and testing. We completed two shots with relatively low anode heating (320 °C) that showed lower loss than the baseline platform. However, we were unable to repeat these results despite several attempts due to a variety of uncontrolled experimental issues, which included hardware fabricated out of concentricity specification, supplier delay in delivering new hardware, and thermal expansion during heating inducing shape and alignment changes. Scaling such a system to Z will require successful demonstration of reproducible and effective plasma mitigation on a Mykonos platform, and then substantial engineering and investment to scale such a system to Z. Managing hardware thermal expansion while keeping anode-cathode gaps within specification with heated electrodes will be challenging in the Z geometry of Figure 1.

The *in situ* plasma discharge cleaning system demonstrated promising experimental results. It was shown that design features like insulating breaks, the ASW HV actuator, and a modified vacuum pumpdown process did not adversely affect the performance of the Mykonos accelerator. The plasma cleaning process was demonstrated to delay formation of electrode plasma and increase the effective impedance of the Mykonos load, as observed by optical and electrical diagnostics. The Mykonos parallel plate platform produces lineal current densities of the same order as the inner MITL at Z and inspires confidence that observables associated with *in situ* cleaning could be repeated there. This work, when combined with previous ASW infrastructure development at Z, supports our assertion that the path forward is low-risk to enable *in situ* cleaning with an optimized and informed discharge cleaning protocol on Z experiments, and is attainable within two years.

REFERENCES

[1] D. B. Sinars *et al.*, "Review of pulsed power-driven high energy density physics research on Z at Sandia," Phys. Plasmas, vol. 27, no. 7, 2020.

[2] W. A. Stygar et al., "55-TW magnetically insulated transmission-line system: Design, simulations, and performance," Phys. Rev. Spec. Top. - Accel. Beams, vol. 12, no. 12, pp. 1–19, 2009.

[3] T. W. Sanford, *et al.*, "Measurement of electron energy deposition necessary to form an anode plasma in Ta, Ti, and C for coaxial bremsstrahlung diodes." Journal of Appl. Phys., 66, 10, 1989.

[4] M. R. Gomez et al., "Experimental study of current loss and plasma formation in the Z Machine post-hole convolute," Phys. Rev. Accel. Beams, vol. 20, no. 1, pp. 1–21, 2017.

[5] E. McCafferty and J. P. Wightman, "Determination of the Concentration of Surface Hydroxyl Groups on Metal Oxide Films by a Quantitative XPS Method," Surface and Interface Analysis, 26, 549–564, 1998.

[6] M. E. Cuneo, "The effect of electrode contamination, cleaning, and conditioning on high-energy pulsed-power device performance." IEEE Transactions on Dielectrics and Electrical Insulation vol 6, 4, 469-485, 1999.

[7] M. E. Cuneo, *et al.*, "Results of vacuum cleaning techniques on the performance of LiF field-threshold ion sources on extraction Applied-B ion diodes at 1-10 TW." IEEE Transactions on Plasma Science, vol 25, 2, 229 – 251, 1997.

[8] B. T. Hutsel *et al.*, "Millimeter-gap Magnetically Insulated Transmission Line power flow experiments," 2015 IEEE Pulsed Power Conf., pp. 1–5., 2015.

[9] B. T. Hutsel, *et al.*, "Current Loss in 0.1 – 100 TW Vacuum transmission lines: experiments and simulations," Sandia National Laboratories Report, SAND2018-10474, 2018.

[10] H. C. Hseuh, *et al.* "Glow discharge cleaning of stainless steel accelerator beam tubes." Journal of Vacuum Science and Technology A, 3, 518 – 522, 1985.

[11] D. Lamppa, *et al.* "The development and characterization of an *in situ* plasma cleaning system for Sandia's Z Machine", Sandia National Laboratories Report, SAND2016-11730, 2016.

[12] W. A. Stygar, *et al.*, "Energy loss to conductors operated at lineal current densities ≤ 10MA/cm: Semianalytic model, magnetohydrodynamic simulations, and experiment." Phys. Rev. Special Topics Accel. Beams, 11, 120401, 2008.

[13] N. Bennett, *et al.*, "Current transport and loss mechanisms in the Z accelerator," Phys. Rev. Accel. Beams, 22, 120401, 2019.

[14] N. Bennett, *et al.* "Magnetized particle transport in multi-MA accelerators." Phys. Rev. Accel. Beams, 24, 060401, 2021.

[15] D. R. Welch, *et al.,* "Electrode contaminant plasma effects on 10^7-A Z pinch accelerators." Phys. Rev. Accel. Beams, 22, 070401, 2019.

[16] "CHICAGO - Plasma Simulation Software." [Online]. Available: http://www.vosssci.com/products/chicago/chicago.html.

[17] J. R. Young, "Outgassing characteristics of stainless steel and aluminum with different surface treatments," J Vac. Sci. Technol., vol. 6, no. 3, pp. 398–400, 1969.

[18] Y. T. Sasaki, "A survey of vacuum material cleaning procedures: A subcommittee report of the American Vacuum Society Recommended Practices Committee," J. Vac. Sci. Technol. A Vacuum, Surfaces, Film., vol. 9, no. 3, pp. 2025–2035, 1991.

[19] S. C. Simpson, *et al.*, "In Vacuo Heating Experiments on Mykonos: A Path Forward to Improving Power Flow on Z," Sandia National Laboratories Report, SAND2021-0869, 2021.

[20] G. R. Laity, *et al.*, "Towards predictive plasma science and engineering through revolutionary multi-scale algorithms and models, final report." Sandia National Laboratories Technical Report, SAND2021-0718, 2021.

APPENDIX A. *IN SITU* HEATING THEORY AND BACKGROUND

All metal substrates have some degree of "contamination" present within their bulk and upon their surface. This contamination may be inherent during manufacturing, fabrication and machining, exposure to chemicals or air, or due to handling. As shown in Figure 2, this contamination of an electrode surface manifests itself as varying layers of oxides, nitrides, adventitious carbon, hydroxyls, and carbonyls bound to the surface. For 304L stainless steel, there are varying amounts of hydrogen and nitrogen present in the material bulk. One approach for removing both the surface and bulk contaminants of electrodes is to employ *in situ* heating while under high vacuum. The following is a brief overview of how we established a temperature requirement for electrode conditioning, as well as characterizing the bulk and surface inventories to help assess and improve our PIC simulation capabilities. A more detailed report is provided in [19]and [20].

Assuming that the parasitic losses within the MITLs are dominated by hydrogen [4]**,** a minimum temperature to deplete the hydrogen inventory can be determined. Temperature Programmed Desorption (TPD) allowed for a direct measurement of outgassing of each species as a function of temperature. For this, a small sample of the electrode (~1 cm^2) is thermally ramped at 1-10 °C /s under ultra-high vacuum (<10^{-9} torr) while using a Residual Gas Analyzer (RGA) to characterize the desorbed species such as CO, CO_2, CH_4, H_2O, H_2. (Note: these desorbed species are the result of chemical reactions/reductions of C, O, and H resulting in a gaseous molecule at the surface). The desorption spectra for a representative 304L stainless steel coupon heated to ~1000 °C [20] is depicted in Figure 25. From this data, it is evident that most contaminants are desorbed by 500 °C – which is in good agreement with the findings in Ref. [18]. An initial temperature of 450 °C was established based off these measurements as the target bakeout temperature to deplete contaminant inventories from the surface and the bulk.

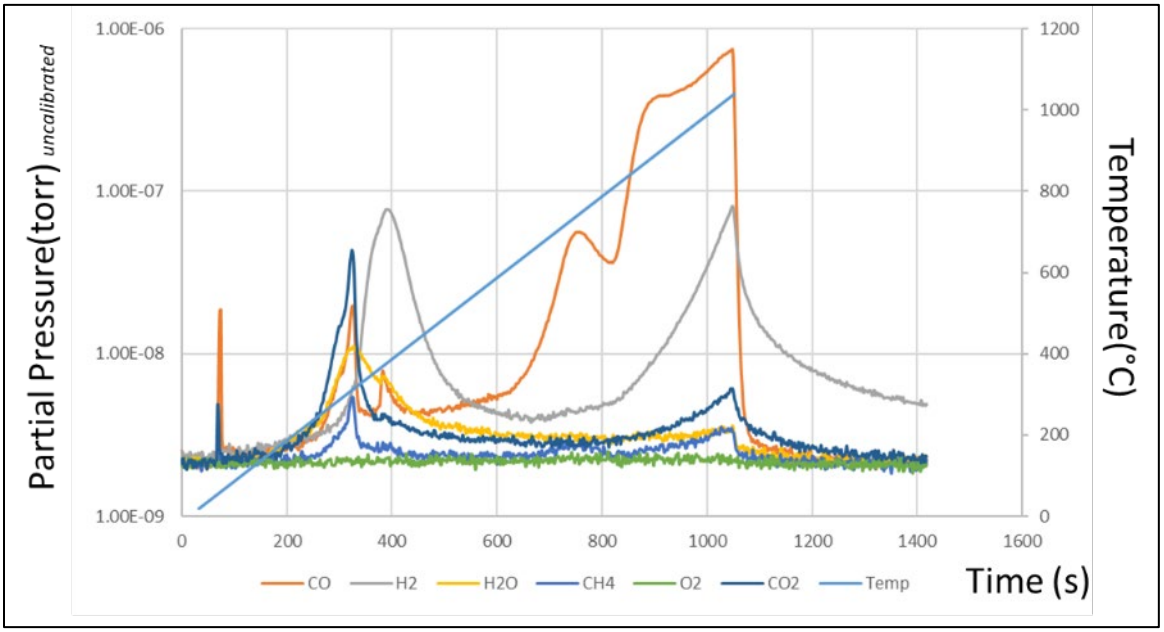

Figure 25: Desorption profile of various contaminants from an untreated 304L stainless steel coupon using TPD. The left axis is given in uncalibrated partial pressure (Torr), the bottom axis is the Temperature of the sample (ºC) or the time (s), and the right axis shows the programmed temperature (ºC) for the linear 'blue' line. Increased desorption of each species at T > 800 °C is most likely a result of background desorption from the chamber walls of the TPD system.

Next, by using calibrated leak sources for each species, it is possible to apply a gauge correction factor for the RGA and quantify the number of monolayers of each species as shown in Table 3. These values can then be compared to and incorporated into the initial boundary conditions used in the CHICAGO PIC [16] simulations of the *in situ* heated hardware and provide an upper boundary for total inventory.

Table 3: Measured inventories of desorbed gasses from a 304L stainless steel coupon using TPD. 1 ML ≈ 10^{15} surface atoms/cm^2 [19]

	Number of Desorbed Monolayers				
	Water (ML)	CO2(ML)	CO (ML)	H2(ML)	Total Coverage
304L	6.8	2.3	50.7	4.5	64.3

Since TPD is unable to distinguish the origins of the desorbed species, X-ray photoelectron spectroscopy (XPS) [5] was employed during the GC LDRD [20] to estimate the initial surface inventories of adsorbed contaminants on a typical 304L stainless steel surface and then subsequently demonstrate the complete reduction of all surface bound hydrogen compounds for a modest 250 °C bakeout. A summary of the estimated coverages is provided in Table 4. These measurements were incorporated to this recent work in two ways: (i) these results clearly demonstrate that a nominal temperature of 250 °C is adequate for reducing all weakly dissociated water (0.3 ML) and all hydroxyls (2.2 ML) from the surface (*see* Table 4 "OH") resulting in a remaining inventory of 8.6 ML of carbon compounds on the surface (i.e. dissociated CO_x and C-C & C-H), and (ii) these results set an upper boundary on the available contaminant inventory at room temperature and 250 °C to be used in the PIC simulations for comparison to experimental results.

Table 4: Results using XPS to estimate the surface coverage of various adsorbates on 304L stainless steel at room temperature and after a 250 °C bakeout. (1 ML ≈ 10^{15} surface atoms/cm^2) [20]

Adsorbed Species	UHV (room temp)	UHV @ 250°C	Desorbed (20 – 250°C)
CO	1 ML	0.5 ML	0.5 ML
CO2	2 ML	1.7 ML	0.3 ML
H_2O	0.3 ML	0 ML	0.3 ML
OH	2.2 ML	0 ML	2.2 ML
C (C-C or C-H)	8 ML	6.4 ML	1.6 ML
Total			**4.9 ML**

APPENDIX B. AUDIO SQUARE-WAVE (ASW) BACKGROUND

A plasma cleaning process aims to remove contaminant particles from a material surface through physical sputtering and/or chemical gettering. Physical sputtering utilizes a heavy inert gas species (like argon) to transfer energy to contaminant molecules adsorbed onto target surfaces. A chemical gettering process uses a chemically reactive gas species like oxygen to bond with liberated atoms and molecules; these reactant products are then mixed into the process gas flow and exhausted via the roughing pump. The gas mixture in all discussed discharge cleaning experiments consists of 80% Argon, 20% oxygen to leverage both phenomena. Contaminants like hydrocarbons and water are bombarded by energetic argon ions, break down into constituent molecules that can react with the oxygen and be pumped out. Research by Hseuh [10] cleaning stainless steel equipment with Argon/Oxygen gas mixtures indicate that a factor of five less ion fluence (total molecules per unit area) is needed to effectively clean a stainless steel surface compared to pure Argon.

Experiments by Tang [11] explored the efficiency of the novel ASW discharge technique for removing known amounts of contaminants from the surfaces of stainless steel coupons. The ASW cleaning technique was shown to be equal to or more effective at removing contaminants than an RF glow discharge excited at 13.56MHz. Removal rates of hydrocarbons (Z Machine oil) and an aerosol-based carbon coating were measured. These contaminants are representative of atomic species whose ion states are thought to contribute to rapid formation of electrode plasma and contribute light ions to parasitic loss mechanisms.

Small steel coupons were inventoried and introduced into the Z load hardware life cycle to sample and cumulatively integrate any contamination that occurs during storage, handling, and installation into the Z vacuum chamber. The contamination constituents of these coupons were studied with several surface interrogation methods like ToF-SIMS – Time-of-Flight Secondary Ion Mass Spectrometry. Some coupons were also characterized before and after a plasma cleaning process to demonstrate how effective the treatment is at removing relevant contaminants.

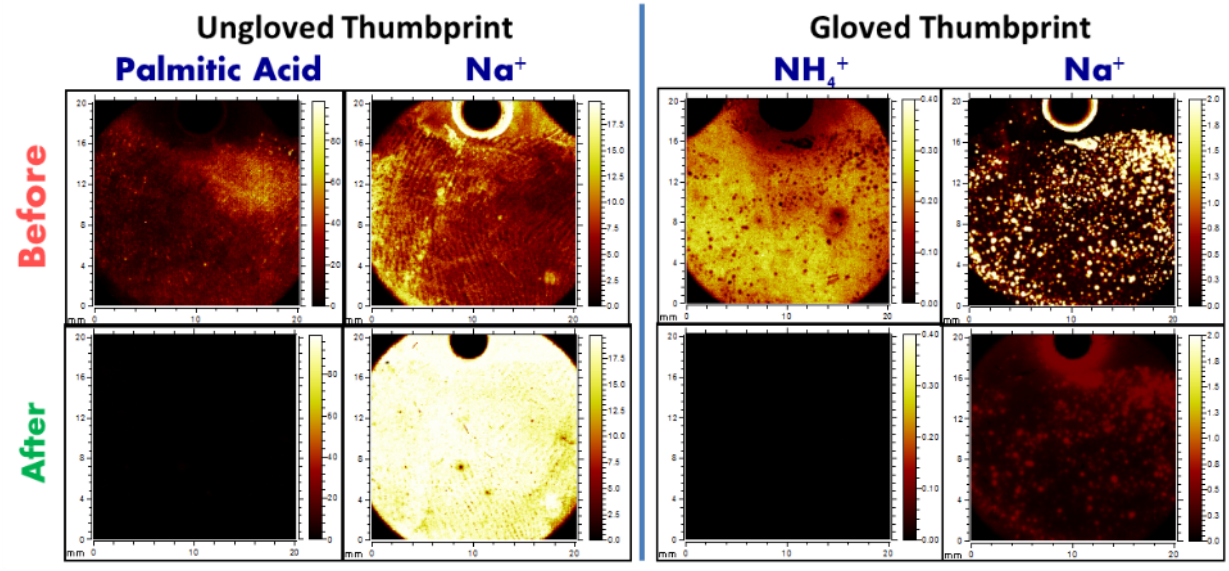

Figure 26: Ten minutes of plasma cleaning had a demonstrable effect at removing organic contaminants like skin and machine oils.

Figure 26 presents some of the most salient results from the previous work. The expected benefit of an *in situ* cleaning process is that it can help forgive many environmental exposures or

mishandling during the hardware lifecycle by removing as much contamination as possible. Figure 26 demonstrates the removal of contamination associated with a gloved and an ungloved thumbprint, both feasible exposures for an accelerator electrode. The ungloved thumbprint observes a near-complete removal of palmitic acid, an organic molecule. The apparent increase in sodium is due to this removal "uncovering" the inorganic metal in the salts left behind. This is acceptable, since a sodium ion is more massive and a slower participant in electrode plasma dynamics. The same occurs with a gloved thumbprint; the ammonium associated with the dry-contact-transferred material is removed, again leaving behind sodium.

The ASW high-voltage driver utilizes a positive- and negative-HV power supply connected to a common transmission line via a fast switching pulser. The switcher is driven by a square wave with frequency selectable between 1 and 50kHz, essentially switching between the HV supplies at audio frequencies. The switching voltage is applied to one of electrode in a low impedance accelerator while the other is grounded. We connect the HV output to the cathode of Z and Mykonos while grounding the anode. This allows the sytsem to leverage the already-grounded anode bulk conductors to complete the circuit and reduce the number of insulating breaks that are needed.

Insulating breaks are needed to isolate the excitation voltage in the regions with smallest gaps, highest power densities, and largest amounts of parasitic current loss. This prevents the power supplies from shorting out to the anode through downstream circuitry. Both Z and Mykonos have water sections that would otherwise terminate the HV output with a load of a few Ohms, which would prevent the supplies from maintaining needed voltages to ionize the process gas.

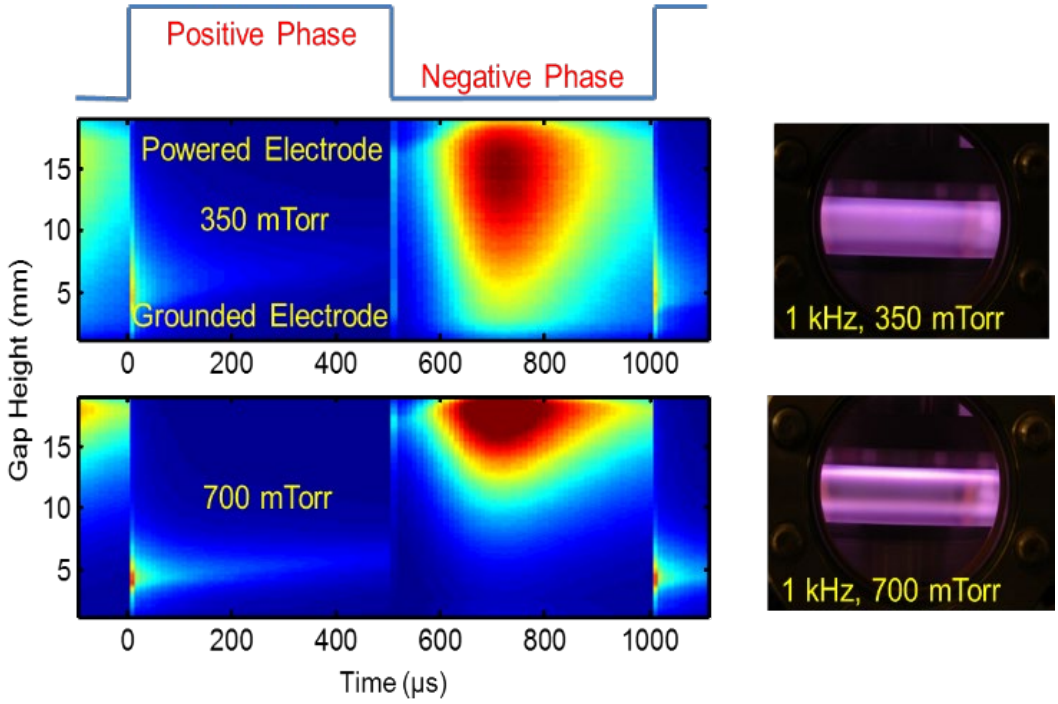

Figure 27: Time-evolution of ASW-excited discharge plasma for two chamber pressures. As pressure increases, the plasma sheath contracts nearer to the electrodes (right). A 1D lineout of such a plasma's during the positive and negative phases of an ASW period shows the time-resolved sheath behavior near powered and grounded electrodes (left) [11].

Figure 27 shows self-emission of a cleaning plasma excited with ASW for two base pressures. As pressure increases, the thickness of the sheath decreases. The plasma sheath is where the electric fields of the excitation can ionize the ions and influence their trajectories; having a sheath of order

the AK gap spacing suggests that ions can be accelerated to sputter the surface of the opposing electrode. The left side of the figure above shows as a function of time a 1D measurement of emission across each gap. When a change of state occurs in the HV wave (noted in the overlaid square waves), the electric field reverses and reforms the sheath near the electrode. The negative phase region generates a more intense plasma near the cathode in this image. For the 350mTorr base pressure, the sheath appears to fill the entire AK gap. It is approximately half for 700mTorr.

The contaminant removal rate of a discharge process is an important parameter to establish such that a recommended cleaning duration may be defined. Experiments early in the ASW research phase [11] used a Residual Gas Analyzer (RGA) to monitor reactant products in the exhaust gas of the plasma process. A test MITL was covered with hand lotion to introduce organic molecules rich in hydrogen, carbon, and oxygen. The MITL was placed in the ASW testbed and a discharge process ran for 45 minutes. The same process was performed with a test MITL that was otherwise clean (no lotion).

The data showed several interesting results:

1) There were reactant products generated on the dirty test sample had a marked increase in partial pressure than for the clean process – it is evident that the discharge plasma is removing the lotion.
2) When the plasmas are ignited at t=0, the process gas oxygen is depleted as reactant products like CO, CO2, and H2O increase – chemical gettering is capturing carbon and hydrogen atoms.
3) The dirty test sample converges to a steady state comparable to the cleaned test in about 20 minutes, suggesting that cleaning process need only be run for half an hour to remove large amounts of intentional contamination.
4) The reactant product background remains for the duration of the plasma cleaning process, but decays once the plasma extinguishes. This is likely due to reactions elsewhere in the vacuum chamber.

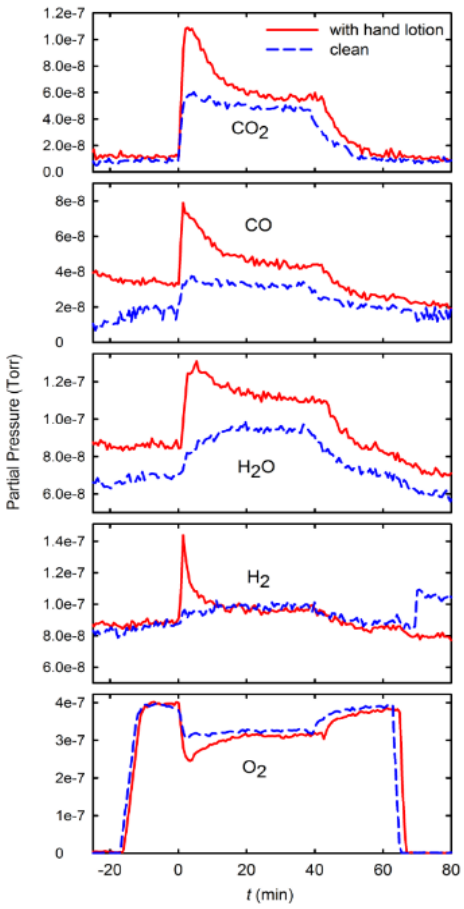

Figure 28: Partial pressures of gas species created during plasma cleaning process. Hand lotion used to initially contaminate the surface.

Future work will include a recontamination process on test electrodes to repeatably refill the inventory of contaminants and estimate removal rates for different conditioning protocols.

The results from this earlier work informed the decision to explore an ASW process for work on the Mykonos experimental facility. ASW excitation of an ArO2 process gas was shown to significantly reduce light atoms like hydrogen, oxygen, and carbon from surfaces of test coupons. It is hypothesized that reducing the inventory of these ion sources will positively affect power flow by delaying electrode plasma formation and its evolution. Experiments on the Mykonos accelerator with ASW will explore this assertion.

APPENDIX C. PIC MODEL OF THE PARALLEL PLATE PLATFORM

The CHICAGO particle-in-cell (PIC) code [16] is used to model the electrode plasma formation in the novel parallel plate MITL section of the Mykonos experiments. These simulations include the main current path electrode hardware for this configuration of the Mykonos front-end. The 3D Cartesian simulation geometry is shown schematically in Figure 29. In this model the "z" direction is along the parallel plate MITL (i.e., the power flow direction), the "x" direction is across the parallel plate AK gap and the "y" direction is transverse to the gap. The model includes one-half load hardware as a symmetry boundary that bisects the simulation model in the y=0 plane. The load is contained within a conducting cylinder. The radius of ~2 cm is sufficient to contain the main electrode hardware and does not significantly influence the electromagnetic fields within the parallel plate MITL section. The experimental configuration modeled is the 2.1 MA/cm lineal current density configuration which is the smallest cathode cross-section fielded, therefore producing the highest current densities on the cathode surface.

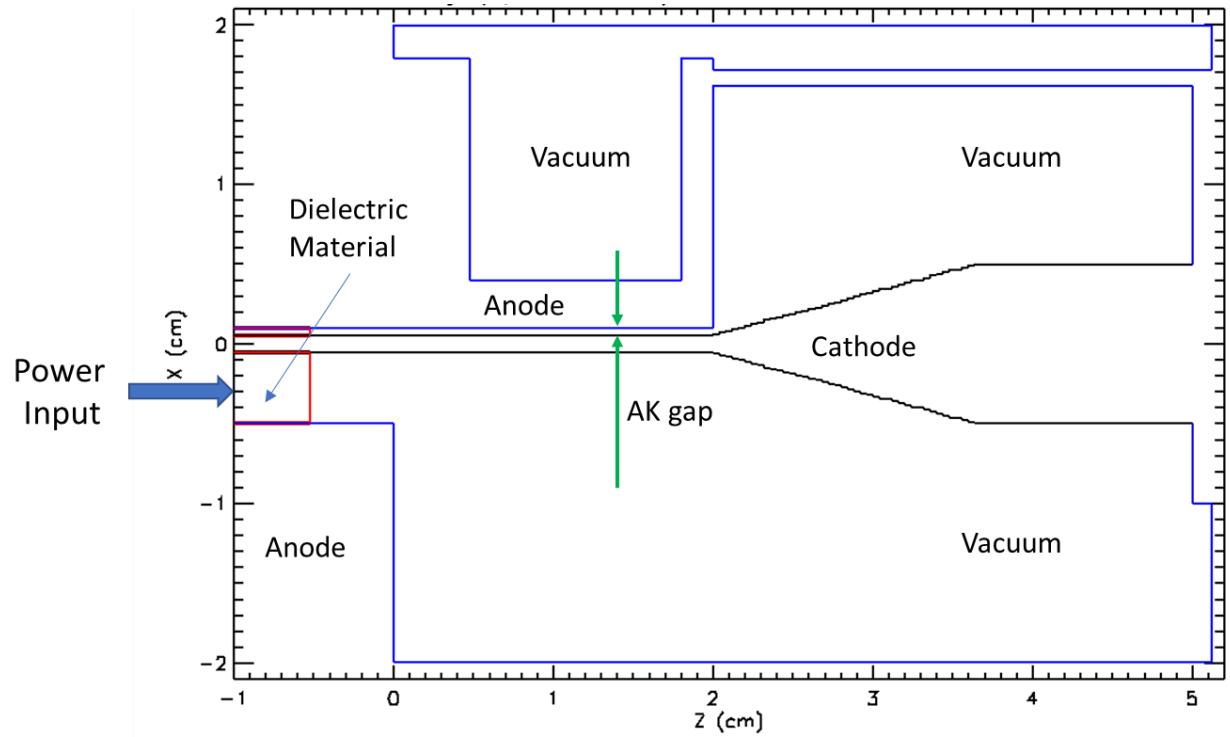

Figure 29: Cross-sectional view (y=0 plane) of the 3D simulation geometry of the Mykonos 2.1 MA/cm lineal current density parallel plate MITL experiment.

The simulations use a simple model for Ohmic heating [13]. In addition, surface heating is also driven by charge particle bombardment. We assume space-charge-limited (SCL) electron emission from the cathode when the local electric field at the conductor surface exceeds 240 kV/cm. Once the anode surface temperature exceeds a temperature increase of 400 °C, SCL emission of ions is enabled. In addition, once these thresholds are met on the electrodes, plasma desorption is initiated with a Temkin-based model [13]. We assume that this plasma is composed of water with an initially uniform coverage on all electrode surfaces in the small-radial coaxial section. These same assumptions are employed in modeling the parallel plate configuration, as well as all experiments on Z.

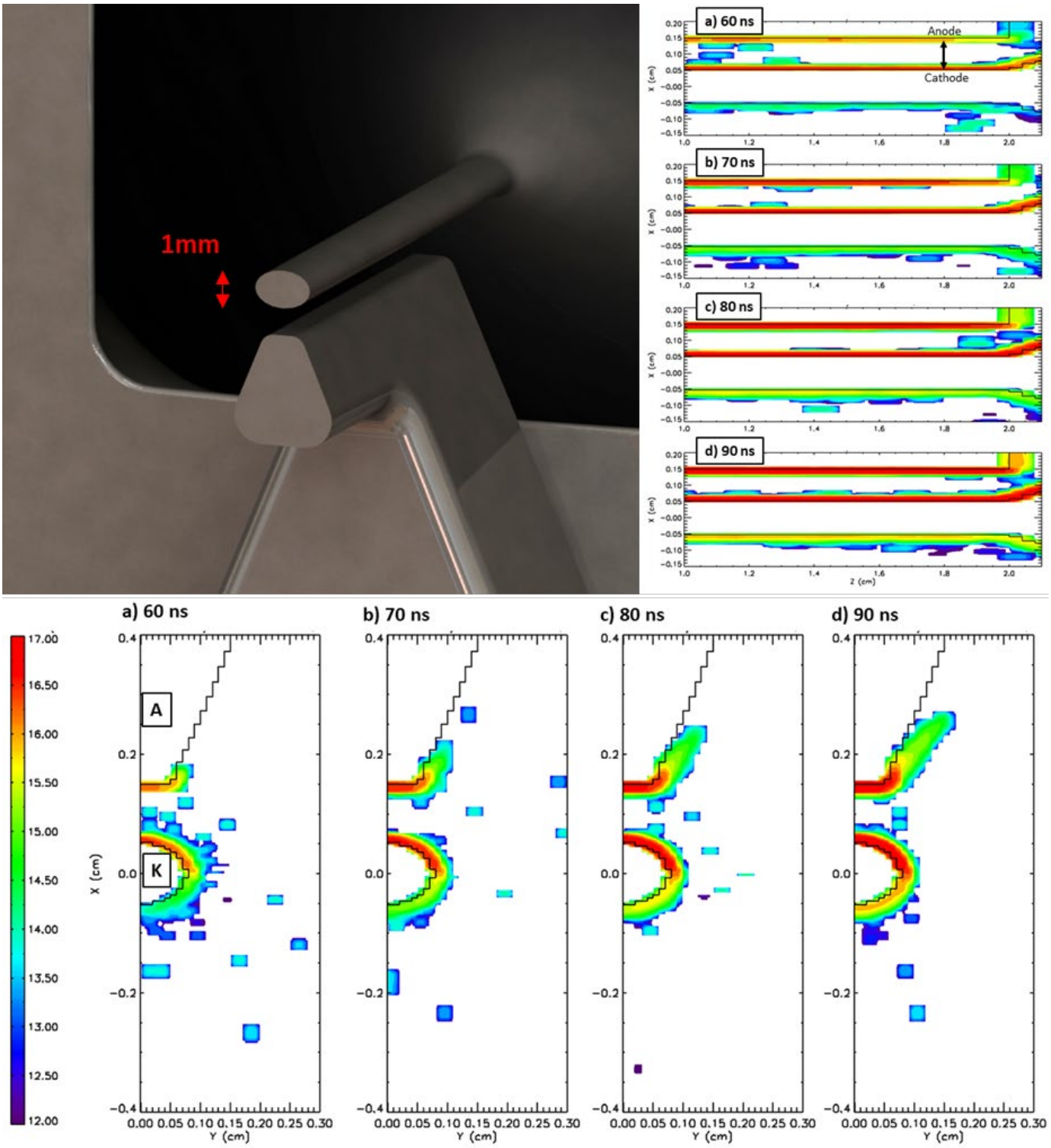

Figure 30: A transverse cross section at the midplane of the experimental MITL shows the elliptical cathode cross section, a 0.5mm AK gap, and the anode (top). In (bottom), Chicago PIC calculations show ion density contours (in log10(n)) evolving using the 1.7 MA/cm design point and 1-mm AK gap, at 1cm. Note that the Chicago geometry is upside down with respect to the experimental hardware. The XZ plane is shown in the Upper Right. Emission is not turned on for outer half of electrodes; observed densities are present because of transport from the main AK region along field lines.

We assume that this plasma is composed of water with an initially uniform coverage on all electrode surfaces in the parallel-plate MITL portion of the hardware. Note that in Figure 30, the simulation AK hardware is upside down when compared to the experimental hardware.

An xy-cut is shown in Figure 30 with both the Solidworks model and the equivalent (inverted geometry) in Chicago. Log-density plots of ion density show the formation of the electrode plasma in the AK gap and subsequent transport along elliptical magnetic field lines (not rendered) out of the anode cathode gap region. This transport provides the plasma around the cathode and anode perimeters; only the inner half of the anode and cathode conductors are permitted to emit charged particles. This behavior is seen in the fast framing images between early- and late-time exposures. This transport mechanism is not present in coaxial geometries because there is no lower-field region for the plasma to push out into. This prevents plasma from accumulating in an enclosed volume and enhancing parasitic current loss. The effect of this has been noted in experiments; parallel plate experiments at AK gaps ~ 0.6 – 0.8 mm have not observed anything like the system current loss in coaxial transmission line experiments with similar AK gaps summarized in the Hutsel vacuum variation experiments [9]. Hutsel presents two shots with his platform and an AK gap of 0.6mm that loses 400kA, as seen in Figure 6. This transport mechanism may be more of a benefit than a hindrance by inhibiting gap closure, preventing a catastrophic current shunt that would normally otherwise occur, and allowing plasma to evolve longer for diagnostic observation.

The Chicago modeling efforts allowed us to compare nominal 0.5- and 1.0-mm self-emission plasma images to notional synthetic images generated by integrating electrode plasma in the y-direction (out of the page in Figure 29 or Figure 31, right). This figure shows a comparison of two uncleaned experiments (left) and the synthetic total ion density (O^+ and H^+) plots from Chicago on the right, as integrated from the midplane outward. The experimental data are simply based on self-emission intensity. Both sets of images include purple lines to show the maximum extent of electrode material before current began to flow. The cathode is on top and the anode is on bottom in the real

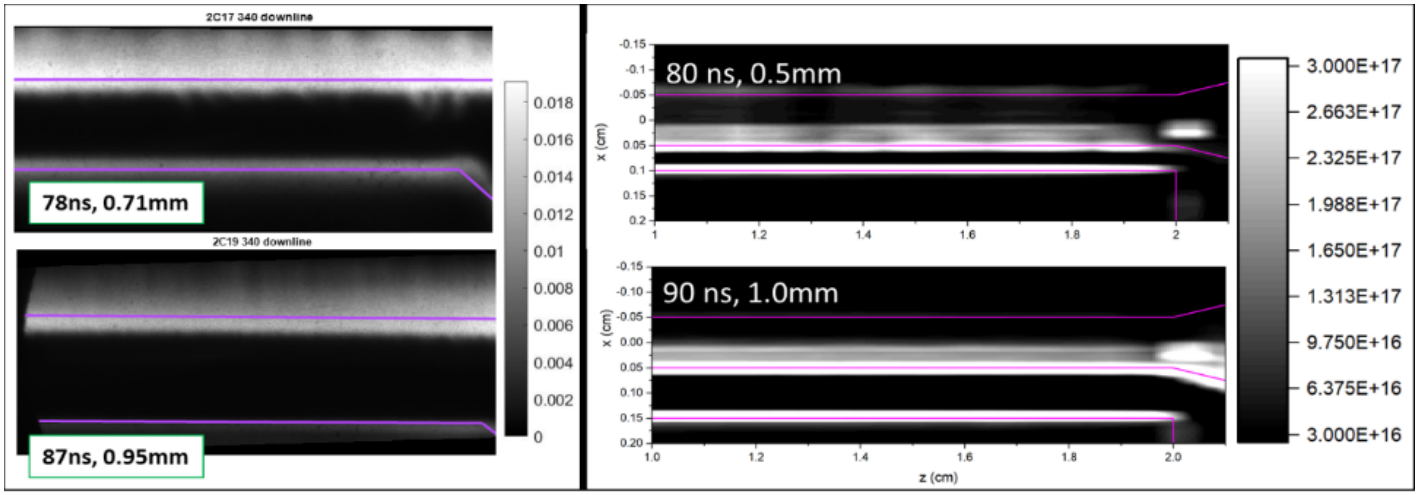

Figure 31: ICCD images for 0.7 and 1.0mm experiments (left) and plasma densities calculated from Chicago PIC calculations for the MP3 platform (right) for 0.5mm and 1.0mm AK gaps. Simulations suggest that electrode plasma turn-on is insensitive to gap spacing, though narrower gaps have higher magnetic fields to increase MRT instability growth rate. These trends are experimentally observed.

and synthetic data. The purple lines can be interpreted as the dark edges of the cathode and anode electrodes being backlit, like the fiducial image shown in Figure 11.

Although this compares intrinsically different data, there are two valuable inferences to make:

1) Instability growth rates that perturb plasma density appear to correlate with narrower gaps. Spatial variation in both experimental and simulated data (top row) supports this assertion.
2) Plasma densities are being achieved that are of the same order regardless of AK gap, as observed in the simulated images. This is encouraging because it suggests that plasma formation processes are less sensitive to the gap.

APPENDIX D. PIC MODEL FOR IN SITU HEATING

The CHICAGO Multiphysics code is used to model the electrode plasma formation in the small-radius coaxial MITL section of the Mykonos experiments. These simulations use a highly idealized configuration of the Mykonos front-end hardware to reduce the simulation volume being modeled while retaining the details of the critical sections of the coaxial transmission line. The 2D (r,z) simulation geometry is shown schematically in Figure 32.

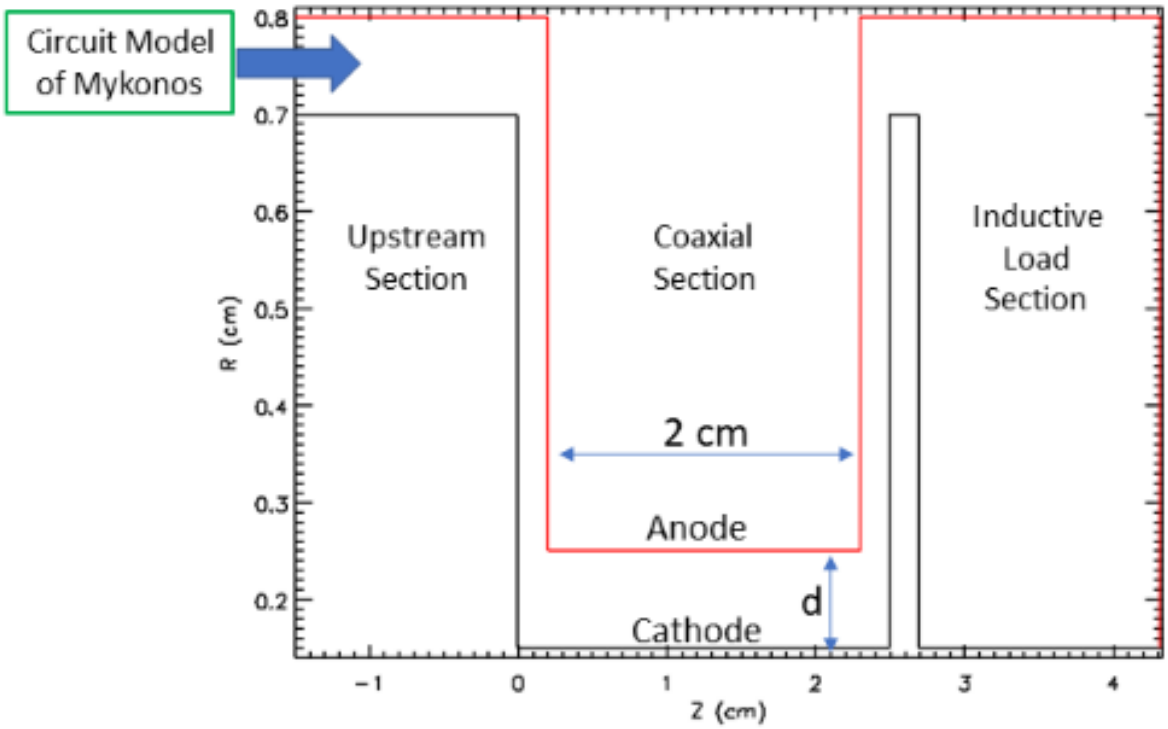

Figure 32: Idealized 2D (r,z) simulation geometry of the Mykonos high current density coaxial MITL experiments.

There are three main axial sections to the simulation model. The upstream section provides a larger-radius coaxial transmission line section to which is connected an equivalent circuit model of the Mykonos generator. This approximates the actual upstream Mykonos hardware, which is roughly a conic transmission line. A constant gap radial transmission line connects the large-radius coaxial upstream section to the small-radius coaxial section in Figure 32. This small radius section is where charged particle creation is enabled. At the end of the small-radius coaxial section, another constant gap radial transmission line drives the inductive load section. No charged particle emission is enabled in the upstream or inductive load sections. Surface heating models are invoked as described in Appendix C.

This page left blank

DISTRIBUTION

Email—Internal

Name	Org.	Sandia Email Address
Derek Lamppa	01659	dclampp@sandia.gov
Sean Simpson	01659	scsimps@sandia.gov
Brian Hutsel	01651	bthutse@sandia.gov
George Laity	01659	grlaity@sandia.gov
Michael Cuneo	01650	mecuneo@sandia.gov
Technical Library	01977	sanddocs@sandia.gov

Email—External [redacted]

Name	Company Email Address	Company Name
David Rose	davidr@vosssci.com	Voss Scientific

Hardcopy—Internal

Number of Copies	Name	Org.	Mailstop
5	Derek Lamppa	01659	1195

This page left blank

Sandia National Laboratories

Sandia National Laboratories is a multimission laboratory managed and operated by National Technology & Engineering Solutions of Sandia LLC, a wholly owned subsidiary of Honeywell International Inc. for the U.S. Department of Energy's National Nuclear Security Administration under contract DE-NA0003525.